Composite Structures 160 (2017) 152–168

Contents lists available at ScienceDirect

Composite Structures

journal homepage: www.elsevier.com/locate/compstruct

Vibration and buckling analysis of double-functionally graded Timoshenko beam system on Winkler-Pasternak elastic foundation

Hao Deng *, KaiDong Chen, Wei Cheng, ShouGen Zhao

School of Aeronautic Science and Engineering, Beihang University, Beijing 100191, China

ARTICLE INFO

Article history:
Received 9 August 2016
Revised 10 October 2016
Accepted 11 October 2016
Available online 19 October 2016

Keywords:
Vibration and buckling
Double-beam system
Dynamic stiffness method
Functionally graded Timoshenko beam
Dynamic characteristic

ABSTRACT

To acquire exact solutions of double-functionally graded Timoshenko beam system on Winkler-Pasternk elastic foundation, which are benchmarks of double-beam systems in the field of engineering, motion differential equations of double-beam system are derived using Hamilton's principle. In this paper, the exact dynamic stiffness matrix of double-functionally graded Timoshenko beam system on Winkler-Pasternak under axial loading are established and the damping of the connecting layer is also taken into consideration. The exact natural frequency and buckling load are obtained using Wittrick-William algorithm. To comprehensively analyze dynamic characteristics of double beam system, the effect of gradient parameter, foundation parameters, axial loading and connecting stiffness on the frequency and buckling load is compared, and the influence of damping factor is also investigated. Finally, dynamic response of double-beam system is studied using Fourier transformation.

1. Introduction

Functionally graded material [1–6] is a combination of two or more than two different properties of material according to a certain law. Two sides of the structure are composed of different physical properties to make the material components meet the special requirements of different conditions. The volume fraction of the component varies continuously in space. The mechanical properties of the structure can vary continuously at different position. Thus, the mutation of physical properties can be eliminated. Meanwhile, FGM can also reduce or avoid the stress concentration phenomenon in the components. Functionally graded materials have the characteristics of high strength, toughness, high temperature resistance and corrosion resistance, which also solves the problem that uncoordination of thermal expansion coefficient between the metal and ceramic. Functionally graded materials have presented the excellent performance in high strength, mechanical load, thermal load, or under high temperature environment. Therefore, FGM is considered as the most potential composite material in the fields of spacecraft, machinery industry and nuclear industry, and the research on mechanical behavior of functionally graded materials has become a frontier subject in modern materials science and mechanics.

Free vibration of functionally graded beams was analyzed by Alshorbagy et al. [7] by using finite element method. Xiang and Yang [8] used direct analytical method to analyze the vibration of a laminated FGM Timoshenko beam. Zhu H [9] used the Fourier series-Galerkin method to investigate the functionally graded beams. Su H [10] acquired the exact solutions of the functionally graded Timoshenko beam using dynamic stiffness method. Thai HT [11] analyzed the bending and free vibration of FGB by using various higher-order shear deformation beam theories. Lai SK [12] has investigated the large amplitude vibration of FGB through accurate analytical perturbation method. Huang Y [13] used a new approach to analyze the free vibration of axially functionally graded beams with non-uniform cross section. A large amount of studies have been done about the beam resting on the Winkler-Pasternak elastic foundation. Lee [14] studied the free vibrations of non-uniform beams resting on two-parameter elastic foundation. Wang [15] acquired the exact solutions for Timoshenko beams on elastic foundations by using Green functions. De Rosa [16] investigated the influence of Pasternak soil on the free vibration of Euler beams. Chen W Q [17] used a mixed method to analyze bending and free vibration of beams resting on a Pasternak elastic foundation. Ying J [18] obtained the two-dimension elasticity solutions for functionally graded beams resting on elastic foundations. In recent years, some higher-order shear deformation theories and normal deformation theory were proposed. M Bourada [19] developed a simple and refined trigonometric

* Corresponding author.
E-mail address: dh4525241@buaa.edu.cn (H. Deng).

http://dx.doi.org/10.1016/j.compstruct.2016.10.027
0263-8223/

higher-order beam theory to analyze bending and vibration of functionally graded beams. H Hebali [20] developed a new quasi-three-dimensional hyperbolic shear deformation theory for the bending and free vibration analysis of functionally graded plates. M Bennoun [21] applied a new five-variable refined plate theory for the free vibration analysis of functionally graded sandwich plates. SA Yahia [22] developed various higher-order shear deformation plate theories for wave propagation in functionally graded plates. Z Belabed [23] proposed an efficient and simple higher order shear and normal deformation theory for functionally graded material plates. A Mahi [24] developed a new hyperbolic shear deformation theory for bending and free vibration analysis of isotropic, functionally graded, sandwich and laminated composite plates. A Hamidi [25] presented a simple but accurate sinusoidal plate theory for thermomechanical bending analysis of functionally graded sandwich plates. High-order beam theories are able to represent the section warping in the deformed configuration and have higher accuracy for high order modes, while acquiring the exact solutions is complex and difficult. For simplicity, Timoshenko beam theory is considered in this paper. Timoshenko beam theory requires shear correction factors and is suitable for composite beams for which the shear correction factors can be determined.

Double-beam system which consists of two parallel beams connected by elastic layer is an important technological extension in industrial field such as double-beam cranes, double-beam spectrometers, double-beam interferometers, etc. Double-beam systems are elements of various devices as well as of mechanical, civil, and aircraft structures. Examples also include aircraft wing spars, double-beam cranes, railway tracks resting on a foundation, bridge spans, pipelines, and trusses. Twin beams can also be encountered in mechanical systems on a smaller scale, for example linear guideways used in plotters or during such technological processes as cutting. Meanwhile, two-beam system such as floating-slab tracks is widely used to control the vibration from underground trains. Functionally graded material can resist high temperature and reduce stress concentration phenomenon, which has a wide range of applications in the high-temperature environment. Therefore, functionally graded double beam system has a broad prospect of application.

S. Kukla [26] studied the free vibration of the two-beam system connected by many translational springs. Z. Oniszczuk [27] studied the free vibration of elastically connected simply supported double-beam complex system. Recently the double-beam system has been used as a new type of vibration absorber to control the vibration of a beam-type structure. Aida [28] et al. analyzed the vibration control of beams by using two-beam system. Hussein [29] modeled floating-slab tracks by using two-beam system and the layer was simulated by the springs and dampers. Shamalta M [30] analyzed the dynamic response of an embedded railway track by analytical method. Zhang et al. [31] investigated the vibration and buckling of a double-beam system under compressive axial loading. Jun Li [32] established an exact dynamic stiffness matrix to compute the natural frequency for an elastically connected three-beam system, which is composed of three parallel beams of uniform properties with uniformly distributed-connecting springs among them. Ariei A [33] studied the transverse vibration of a multiple-Timoshenko beam system with intermediate elastic connections. Simsek M [34] et al. studied nonlocal effects in the forced vibration of an elastically connected double-carbon nanotube system. Palmeri [35] used a novel state-space form to study transverse vibrations of double-beam systems made of two outer elastic beams continuously joined by an inner viscoelastic layer. M. Abu [36] studied the dynamic response of a double Euler-Bernoulli beam under a moving constant load. W.-R [37] has investigated bending vibration of axially loaded Timoshenko beams with locally distributed Kelvin-Voigt damping. Recently, Simsek [38] studied the dynamics of elastically connected double-functionally graded beam systems with different boundary conditions under action of a moving load based on the Euler beam theory.

As mentioned earlier, these studies primarily focused on beam system made of homogeneous material. Inhomogeneous material, such as functionally graded material, is rarely involved. At the same time, main solution method these studies based on depends on numerical solution, such as finite element method, but the precision of numerical method cannot be gauranteed. Thus, it is essential to acquire exact solutions which can be benchmarks of double-beam systems made of functionally graded materials. Elastic foundation model can be used to simulate the interactions between beam system and elastic medium, B Bouderba [39] delt with the thermomechanical bending response of functionally graded plates resting on Winkler-Pasternak elastic foundations. Meziane [40] presented an efficient and simple refined shear deformation theory for the vibration and buckling of exponentially graded material sandwich plate resting on elastic foundations under various boundary conditions. M Zidi [41] studied the bending response of functionally graded material plate resting on elastic foundation. ND Duc [42] investigated the nonlinear dynamic response of eccentrically stiffened functionally graded double curved shallow shells resting on elastic foundations. ND Duc [43] studied the nonlinear response of thick functionally graded double-curved shallow panels resting on elastic foundations and subjected to thermal and thermomechanical loads. ND Duc [44] studied the nonlinear response of panels resting on elastic foundations, which account for higher order transverse shear deformation and panel-foundation interaction. ND Duc [45] studied nonlinear response of imperfect eccentrically stiffened FGM cylindrical panels on elastic foundation subjected to mechanical loads. ND Duc [46] developed an analytical approach to investigate the nonlinear static buckling and post-buckling for imperfect eccentrically stiffened functionally graded thin circular cylindrical shells surrounded on elastic foundation with ceramic–metal–ceramic layers. ND Duc [47] analyzed nonlinear stability of the imperfect FGM cylindrical panel reinforced by eccentrically stiffeners on elastic foundations. ND Duc [48] investigated the linear stability analysis of eccentrically stiffened FGM conical shell panels reinforced by mechanical and thermal loads on elastic foundation. ND Duc [49] used third shear deformation shell theory to investigate nonlinear thermal dynamic behavior of imperfect functionally graded circular cylindrical shells eccentrically reinforced by outside stiffeners and surrounded on elastic foundations. Recently, Duc ND [50] studied nonlinear thermo-electro-mechanical dynamic response of shear deformable piezoelectric Sigmoid functionally graded sandwich circular cylindrical shells on elastic foundations. However, the studies about the double-functionally graded beams system resting on Winkler-Pasternak elastic foundations are very rare. Because of the widely application of functionally graded Timoshenko beam in engineering field, the author formulates the exact dynamic stiffness matrix of the two-beam system resting on Winkler-Pasternak elastic foundation under the axial loads, and the damping of connection layer is also taken into consideration when analyzing the dynamic response of the structure. Finally, buckling of double-functionally graded Timoshenko beam system is also analyzed. The concept of the dynamic stiffness matrix method was first proposed by Kolousek [51] in the early 1940 s. This method is a powerful tool to solve the problem of structural vibration in engineering, especially in the need to obtain higher order natural frequency and higher accuracy. The dynamic stiffness matrix method [52–58] is also commonly referred to as an exact method. Thus, the dynamic stiffness matrix of the two-beam system is established to analyze the effect of parameters on dynamic characteristic and buckling of the system.

2. Theory and formulation

2.1. 1motion differential equations

Fig. 1 shows that the two functionally graded Timoshenko beams are connected by the elastic connection. This two-beam system rests on the elastic foundation under axial forces N. The Winkler elastic layer between the two beams can be simulated by the tension spring, and the spring stiffness of per unit length is K. The elastic foundation is made of two layers which are Winkler layer and shearing layer. The two functionally graded Timoshenko beams have the same length L, width b and thickness h. Assuming that the material properties of the two beams are the same, and the material properties are elastic modulus $E(z)$, shear modulus $G(z)$, poisson's ratio v and mass density $\rho(z)$. For the common FGM beam, the bottom surface is made of metal materials and the top surface is made of ceramic materials. The middle part of beam is the mixture of two materials. Because the values of possion's ratio v of metal materials and ceramic materials are close, the Poisson's ratio v of the beam is regarded as a constant value. And the material properties varying along the thickness direction satisfy power-law [1] form except for poisson's ratio v. Therefore, the properties of the functionally graded Timoshenko beam need to satisfy:

$$P(z) = (P_t - P_b)V_t + P_b \tag{1}$$

where $P(z)$ is the material property including elastic modulus, shear modulus and mass density. P_t is the property at the top surface, and

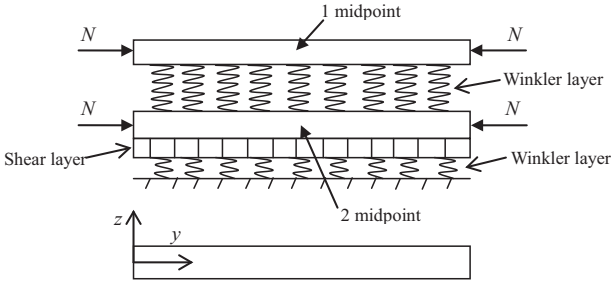

Fig. 1. An elastically connected double-functionally graded Timoshenko beam system on the elastic foundation under the axial forces.

P_b is the properties at the bottom surface. where V_t is the volume fraction of material component. Assuming the origin of coordinates is established on the central axis of the functionally graded Timoshenko beam, volume fraction V_t which is the power function along the thickness direction can be given by power-law [1]:

$$V_t = \left(\frac{z}{h} + \frac{1}{2}\right)^k (k \geqslant 0) \tag{2}$$

where k is the gradient index. Fig. 2 shows the influence of gradient index k on the volume fraction V_t.

According to the theory of functionally graded Timoshenko, v and w are the displacements of the point on the neutral axis along the y and z directions. u_y andu_z are the displacements of the point on the cross section perpendicular to the neutral axis along the y and z directions. Thus,

$$u_y(y,z,t) = v(y,t) - z\phi(y,t) \tag{3}$$

$$u_z(y,z,t) = w(y,t) \tag{4}$$

where ϕ is the bending rotation of the cross-sections. According to the theory of elasticity, the relationship between strain and displacement is given as:

$$\begin{Bmatrix} \varepsilon_{yy} \\ \gamma_{yz} \end{Bmatrix} = \begin{Bmatrix} \frac{\partial u_y}{\partial y} \\ \frac{\partial u_y}{\partial z} + \frac{\partial u_z}{\partial y} \end{Bmatrix} = \begin{Bmatrix} \frac{\partial v}{\partial y} - z \cdot \frac{\partial \phi}{\partial y} \\ \frac{\partial w}{\partial y} - \phi \end{Bmatrix} \tag{5}$$

where ε_{yy} is the normal strains and γ_{yz} is shear strain. According to Hooke's law:

$$\begin{bmatrix} \sigma_{yy} \\ \tau_{yz} \end{bmatrix} = \begin{bmatrix} E(z) & 0 \\ 0 & G(z) \end{bmatrix} \begin{bmatrix} \varepsilon_{yy} \\ \gamma_{yz} \end{bmatrix} \tag{6}$$

where σ_{yy}, τ_{yz} are the normal and shear stresses of the functionally graded Timoshenko beam. Using the above constitutive relationships, the strain energy Π_s and kinetic energy T of double-functionally graded Timoshenko beam systems can be expressed as:

$$\Pi_s = \frac{1}{2}\sum_{i=1}^{2}\int_0^L \left[A_0\left(\frac{\partial v_i}{\partial y}\right)^2 - 2A_1\frac{\partial v_i}{\partial y}\frac{\partial \phi_i}{\partial y} + A_2\left(\frac{\partial \phi_i}{\partial y}\right)^2 + A_3\left(\frac{\partial w_i}{\partial y}\right)^2 - 2\frac{\partial w_i}{\partial y}\phi_i + \phi_i^2\right]dy \tag{7}$$

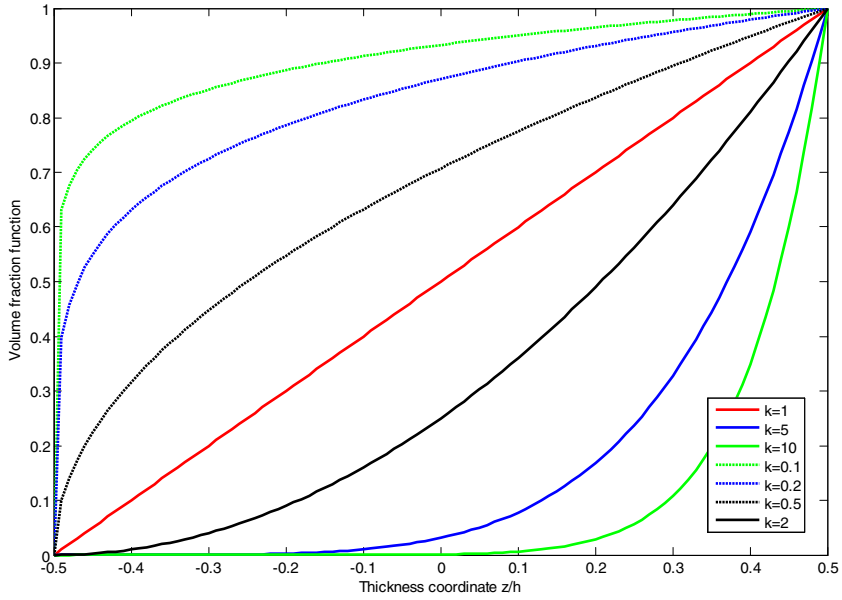

Fig. 2. The effect of the gradient index k on the volume fraction function.

$$T=\frac{1}{2}\sum_{i=1}^{2}\int_0^L\left[I_0\left(\left(\frac{\partial w_i}{\partial t}\right)^2+\left(\frac{\partial v_i}{\partial t}\right)^2\right)-2I_1\left(\frac{\partial v_i}{\partial t}\right)\cdot\left(\frac{\partial \phi_i}{\partial t}\right)+I_2\cdot\left(\frac{\partial \phi_i}{\partial t}\right)^2\right]dy \tag{8}$$

where subscripts 1 and 2 denote the upper beam and lower beam. And

$$\begin{aligned} &I_i=\int z^i\rho(z)dA,\quad A_i=\int z^iE(z)dA(i=0,1,2)\\ &A_3=\int \kappa G(z)dA \end{aligned} \tag{9}$$

where κ is the shear coefficient and$\kappa=5/6$. The work done by axial force$N$ can be expressed as:

$$\Pi_p=\frac{1}{2}\sum_{i=1}^{2}\int_0^L\left[N\left(\frac{\partial w_i}{\partial y}\right)^2\right]dy \tag{10}$$

The elastic potential energy of elastic foundation is donoted by

$$\Pi_f=\frac{b}{2}\int_0^L\left[K_w w_2^2+K_s\left(\frac{\partial w_2}{\partial x}\right)^2\right]dx \tag{11}$$

where K_w, K_s are the parameters of the elastic foundation. Potential energy induced by the elastic layer between the beams can be expressed as

$$U_{el}=\frac{1}{2}\int_0^L K(w_1-w_2)^2dx \tag{12}$$

Hamilton's principle states:

$$\delta\int_{t_1}^{t_2}(T-U_{el}+\Pi_p-\Pi_f-\Pi_s)dt=0 \tag{13}$$

Where t_1 and t_2 are the time interval, and δ is the usual variational operator. The governing differential equations of motion can be obtained by Eq. (13) through the application of symbolic computation:

$$-I_0\ddot{v}_1+A_0v_1''+I_1\ddot{\phi}_1-A_1\phi_1''=0 \tag{14}$$

$$-I_0\ddot{w}_1+A_3w_1''-A_3\phi_1'-K(w_1-w_2)-Nw_1''=0 \tag{15}$$

$$I_1\ddot{v}_1-A_1v_1''+A_3w_1'-I_2\ddot{\phi}_1+A_2\phi_1''-A_3\phi_1=0 \tag{16}$$

$$-I_0\ddot{v}_2+A_0v_2''+I_1\ddot{\phi}_2-A_1\phi_2''=0 \tag{17}$$

$$-I_0\ddot{w}_2+A_3w_2''-A_3\phi_2'+K(w_1-w_2)-Nw_2''+(K_sw_2''-K_ww_2)\cdot b=0 \tag{18}$$

$$I_1\ddot{v}_2-A_1v_2''+A_3w_2'-I_2\ddot{\phi}_2+A_2\phi_2''-A_3\phi_2=0 \tag{19}$$

The axial force F_1, F_2, shear force S_1, S_2 and bending moment M_1, M_2 are obtained as:

$$F_i=-A_0v_i'+A_1\phi_i', S_i=-A_3w_i'+A_3\phi_i, M_i=A_1v_i'-A_2\phi_i';(i=1,2) \tag{20}$$

Assuming harmonic oscillation so that

$$\begin{aligned} v_i(y,t)&=V_i(y)e^{i\omega t},\quad w_i(y,t)=W_i(y)e^{i\omega t},\quad \phi_i(y,t)\\ &=\Phi_i(y)e^{i\omega t}(i=1,2) \end{aligned} \tag{21}$$

where V_i, W_i and Φ_i are amplitudes of v_i, w_i, ϕ_i, and ω is the circular frequency. Differential equations of state space can be obtained by substituting Eq. (21) into Eqs. (14)–(19):

$$\frac{\partial\mathbf{v}}{\partial y}=\mathbf{A}\cdot\mathbf{v} \tag{22}$$

where $\mathbf{v}$ is state space vector, and $\mathbf{v}=[W_1,\Phi_1,V_1,S_1,M_1,F_1,W_2,\Phi_2,V_2,S_2,M_2,F_2]^T$. T denotes transpose and $S_i, M_i, F_i(i=1,2)$ are the amplitudes of shear force, bending moment and axial force.where

$$\mathbf{A}=\begin{bmatrix} 0 & 1 & 0 & a_1 & 0 & 0 & 0 & 0 & 0 & 0 & 0 & 0\\ 0 & 0 & 0 & 0 & a_2 & a_3 & 0 & 0 & 0 & 0 & 0 & 0\\ 0 & 0 & 0 & 0 & a_3 & a_4 & 0 & 0 & 0 & 0 & 0 & 0\\ \frac{a_5}{1-NA_3^{-1}}-K & 0 & 0 & 0 & -\frac{Na_2}{1-NA_3^{-1}} & -\frac{Na_3}{1-NA_3^{-1}} & K & 0 & 0 & 0 & 0 & 0\\ 0 & a_6 & a_7 & -1 & 0 & 0 & 0 & 0 & 0 & 0 & 0 & 0\\ 0 & a_7 & a_5 & 0 & 0 & 0 & 0 & 0 & 0 & 0 & 0 & 0\\ 0 & 0 & 0 & 0 & 0 & 0 & 0 & 1 & 0 & a_1 & 0 & 0\\ 0 & 0 & 0 & 0 & 0 & 0 & 0 & 0 & 0 & 0 & a_2 & a_3\\ 0 & 0 & 0 & 0 & 0 & 0 & 0 & 0 & 0 & 0 & a_3 & a_4\\ K & 0 & 0 & 0 & 0 & 0 & \frac{a_5-K_wb}{1+(K_sb-N)A_3^{-1}}-K & 0 & 0 & 0 & \frac{(K_sb-N)a_2}{1+(K_sb-N)A_3^{-1}} & \frac{(K_sb-N)a_3}{1+(K_sb-N)A_3^{-1}}\\ 0 & 0 & 0 & 0 & 0 & 0 & 0 & a_6 & a_7 & -1 & 0 & 0\\ 0 & 0 & 0 & 0 & 0 & 0 & 0 & a_7 & a_5 & 0 & 0 & 0 \end{bmatrix}$$

where

$$\begin{aligned} &a_1=-A_3^{-1},\quad a_2=\frac{A_0}{A_1^2-A_0A_2},\quad a_3=\frac{A_1}{A_1^2-A_0A_2},\quad a_4=\frac{A_2}{A_1^2-A_0A_2}\\ &a_5=\omega^2I_0,\quad a_6=\omega^2I_2,\quad a_7=-\omega^2I_1 \end{aligned} \tag{23}$$

$\lambda_i(i=1\ldots12)$ are the twelve eigenvalues of matrix **A**. Thus, Eq. (22) can be solved by using differential equation theory:

$$V_i(y)=\sum_{j=1}^{12}P_{ij}e^{\lambda_iy},\quad W_i(y)=\sum_{j=1}^{12}Q_{ij}e^{\lambda_iy},\quad \Phi_i(y)=\sum_{j=1}^{12}R_{ij}e^{\lambda_iy}(i=1,2) \tag{24}$$

where P_{ij}, Q_{ij}, R_{ij} are the constants, and the relationship between the constants can be obtained as:

$$P_{ij}=\alpha_{ij}R_{ij}, Q_{ij}=\beta_{ij}R_{ij}(i=1,2;\ j=1,\ldots12) \tag{25}$$

where

$$\alpha_{ij} = \frac{\omega^2 I_1 + A_1\lambda_j^2}{\omega^2 I_0 + A_0\lambda_j^2}(i = 1,2;\ j = 1,\dots 12) \tag{26}$$

$$\beta_{ij} = \frac{\omega^2 I_2 + A_2\lambda_j^2 - A_3}{\lambda_j A_3 - \omega^2 I_1\alpha_{ij} - \lambda_j^2 A_1\alpha_{ij}}(i = 1,2;\ j = 1\dots 12) \tag{27}$$

And the relationship between R_{1j} and R_{2j} can be obtained through Eq. (15)

$$R_{2j} = \gamma_j R_{1j}(j = 1,\cdots 12) \tag{28}$$

where

$$\gamma_j = \frac{1}{K\beta_{2j}}\left[-\omega^2 I_0\beta_{1j} - \lambda_j^2 A_3\beta_{1j} + A_3\lambda_j + K\beta_{1j} + \lambda_j^2 N_1\beta_{1j}\right] \tag{29}$$

Similarly, the amplitudes of shear force, bending moment and axial force can be obtained by Eq. (19):

$$F_i = -A_0 v_i' + A_1\phi_i' = \sum_{j=1}^{12}(A_1\lambda_j - A_0\lambda_j\alpha_{ij})R_{ij}e^{\lambda_j y}\ (i = 1,2) \tag{30}$$

$$M_i = \sum_{j=1}^{12}(A_1\lambda_j\alpha_{ij} - A_2\lambda_j)R_{ij}e^{\lambda_j y}\ (i = 1,2) \tag{31}$$

$$S_i = \sum_{j=1}^{12}(-A_3\beta_{ij}\lambda_j + A_3)R_{ij}e^{\lambda_j y}\ (i = 1,2) \tag{32}$$

2.2. Dynamic stiffness formulation

The length of functionally graded beam is L. To obtain the dynamic stiffness matrix of two-beam system, the natural boundary conditions for forces and displacements at the end of the beam are applied. According to Fig. 3, the boundary conditions for forces and displacements are:

$$\begin{aligned} &x = 0: W_1 = W_{11},\ W_2 = W_{21},\ \Phi_1 = \Phi_{11},\ \Phi_2 = \Phi_{21}\\ &V_1 = V_{11},\ V_2 = V_{21}\\ &x = L: W_1 = W_{12},\ W_2 = W_{22},\ \Phi_1 = \Phi_{12},\ \Phi_2 = \Phi_{22}\\ &V_1 = V_{12},\ V_2 = V_{22} \end{aligned} \tag{33}$$

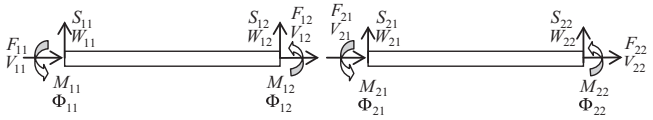

Fig. 3. The boundary conditions for the displacements and forces of the two beam system.

$$\begin{aligned} &x = 0: S_1 = S_{11},\ S_2 = S_{21},\ M_1 = M_{11},\ M_2 = M_{21} F_1 = F_{11},\ F_2 = F_{21}\\ &x = L: S_1 = -S_{12},\ S_2 = -S_{22},\ M_1 = -M_{12},\ M_2 = -M_{22}\\ &F_1 = -F_{12},\ F_2 = -F_{22} \end{aligned} \tag{34}$$

Force vector **F** and displacement vector **d** are defined as:

$$\mathbf{d} = [W_{11}, W_{21}, \Phi_{11}, \Phi_{21}, V_{11}, V_{21}, W_{12}, W_{22}, \Phi_{12}, \Phi_{22}, V_{12}, V_{22}]^T \tag{35}$$

$$\mathbf{F} = [S_{11}, S_{21}, M_{11}, M_{21}, F_{11}, F_{21}, S_{12}, S_{22}, M_{12}, M_{22}, F_{12}, F_{22}]^T \tag{36}$$

Vector **R** is defined as:

$$\mathbf{R} = [R_{11}, R_{12}, R_{13}, R_{14}, R_{15}, R_{16}, R_{17}, R_{18}, R_{19}, R_{110}, R_{111}, R_{112}]^T \tag{37}$$

According to Eqs. (24)–(28), The relationship between **d** and **R** can be expressed as

$$\mathbf{d} = \mathbf{B}\cdot\mathbf{R} \tag{38}$$

where

$$\mathbf{B} = \begin{bmatrix}\mathbf{B}_1\\ \mathbf{B}_2\end{bmatrix} \tag{39}$$

$$\mathbf{B}_1 = \begin{bmatrix} \beta_{11} & \beta_{12} & \beta_{13} & \beta_{14} & \beta_{15} & \beta_{16} & \beta_{17} & \beta_{18} & \beta_{19} & \beta_{110} & \beta_{111} & \beta_{112}\\ \beta_{21}\gamma_1 & \beta_{22}\gamma_2 & \beta_{23}\gamma_3 & \beta_{24}\gamma_4 & \beta_{25}\gamma_5 & \beta_{26}\gamma_6 & \beta_{27}\gamma_7 & \beta_{28}\gamma_8 & \beta_{29}\gamma_9 & \beta_{210}\gamma_{10} & \beta_{211}\gamma_{11} & \beta_{212}\gamma_{12}\\ 1 & 1 & 1 & 1 & 1 & 1 & 1 & 1 & 1 & 1 & 1 & 1\\ \gamma_1 & \gamma_2 & \gamma_3 & \gamma_4 & \gamma_5 & \gamma_6 & \gamma_7 & \gamma_8 & \gamma_9 & \gamma_{10} & \gamma_{11} & \gamma_{12}\\ \alpha_{11} & \alpha_{12} & \alpha_{13} & \alpha_{14} & \alpha_{15} & \alpha_{16} & \alpha_{17} & \alpha_{18} & \alpha_{19} & \alpha_{110} & \alpha_{111} & \alpha_{112}\\ \alpha_{21}\gamma_1 & \alpha_{22}\gamma_2 & \alpha_{23}\gamma_3 & \alpha_{24}\gamma_4 & \alpha_{25}\gamma_5 & \alpha_{26}\gamma_6 & \alpha_{27}\gamma_7 & \alpha_{28}\gamma_8 & \alpha_{29}\gamma_9 & \alpha_{210}\gamma_{10} & \alpha_{211}\gamma_{11} & \alpha_{212}\gamma_{12} \end{bmatrix} \tag{40}$$

Matrix $\mathbf{B}_2$ can be derived as

$$\mathbf{B}_2 = \mathbf{B}_1\cdot\mathbf{E} \tag{41}$$

where

$$\mathbf{E} = [e^{\lambda_1 L}, e^{\lambda_2 L}, e^{\lambda_3 L}, e^{\lambda_4 L}, e^{\lambda_5 L}, e^{\lambda_6 L}, e^{\lambda_7 L}, e^{\lambda_8 L}, e^{\lambda_9 L}, e^{\lambda_{10} L}, e^{\lambda_{11} L}, e^{\lambda_{12} L}]^T \tag{42}$$

Thus

$$\mathbf{B}_2 = \begin{bmatrix} \beta_{11}e^{\lambda_1 L} & \beta_{12}e^{\lambda_2 L} & \beta_{13}e^{\lambda_3 L} & \beta_{14}e^{\lambda_4 L} & \beta_{15}e^{\lambda_5 L} & \beta_{16}e^{\lambda_6 L} & \beta_{17}e^{\lambda_7 L} & \beta_{18}e^{\lambda_8 L} & \beta_{19}e^{\lambda_9 L} & \beta_{110}e^{\lambda_{10} L} & \beta_{111}e^{\lambda_{11} L} & \beta_{112}e^{\lambda_{12} L}\\ \beta_{21}\gamma_1 e^{\lambda_1 L} & \beta_{22}\gamma_2 e^{\lambda_2 L} & \beta_{23}\gamma_3 e^{\lambda_3 L} & \beta_{24}\gamma_4 e^{\lambda_4 L} & \beta_{25}\gamma_5 e^{\lambda_5 L} & \beta_{26}\gamma_6 e^{\lambda_6 L} & \beta_{27}\gamma_7 e^{\lambda_7 L} & \beta_{28}\gamma_8 e^{\lambda_8 L} & \beta_{29}\gamma_9 e^{\lambda_9 L} & \beta_{210}\gamma_{10} e^{\lambda_{10} L} & \beta_{211}\gamma_{11} e^{\lambda_{11} L} & \beta_{212}\gamma_{12} e^{\lambda_{12} L}\\ e^{\lambda_1 L} & e^{\lambda_2 L} & e^{\lambda_3 L} & e^{\lambda_4 L} & e^{\lambda_5 L} & e^{\lambda_6 L} & e^{\lambda_7 L} & e^{\lambda_8 L} & e^{\lambda_9 L} & e^{\lambda_{10} L} & e^{\lambda_{11} L} & e^{\lambda_{12} L}\\ \gamma_1 e^{\lambda_1 L} & \gamma_2 e^{\lambda_2 L} & \gamma_3 e^{\lambda_3 L} & \gamma_4 e^{\lambda_4 L} & \gamma_5 e^{\lambda_5 L} & \gamma_6 e^{\lambda_6 L} & \gamma_7 e^{\lambda_7 L} & \gamma_8 e^{\lambda_8 L} & \gamma_9 e^{\lambda_9 L} & \gamma_{10} e^{\lambda_{10} L} & \gamma_{11} e^{\lambda_{11} L} & \gamma_{12} e^{\lambda_{12} L}\\ \alpha_{11} e^{\lambda_1 L} & \alpha_{12} e^{\lambda_2 L} & \alpha_{13} e^{\lambda_3 L} & \alpha_{14} e^{\lambda_4 L} & \alpha_{15} e^{\lambda_5 L} & \alpha_{16} e^{\lambda_6 L} & \alpha_{17} e^{\lambda_7 L} & \alpha_{18} e^{\lambda_8 L} & \alpha_{19} e^{\lambda_9 L} & \alpha_{110} e^{\lambda_{10} L} & \alpha_{111} e^{\lambda_{11} L} & \alpha_{112} e^{\lambda_{12} L}\\ \alpha_{21}\gamma_1 e^{\lambda_1 L} & \alpha_{22}\gamma_2 e^{\lambda_2 L} & \alpha_{23}\gamma_3 e^{\lambda_3 L} & \alpha_{24}\gamma_4 e^{\lambda_4 L} & \alpha_{25}\gamma_5 e^{\lambda_5 L} & \alpha_{26}\gamma_6 e^{\lambda_6 L} & \alpha_{27}\gamma_7 e^{\lambda_7 L} & \alpha_{28}\gamma_8 e^{\lambda_8 L} & \alpha_{29}\gamma_9 e^{\lambda_9 L} & \alpha_{210}\gamma_{10} e^{\lambda_{10} L} & \alpha_{211}\gamma_{11} e^{\lambda_{11} L} & \alpha_{212}\gamma_{12} e^{\lambda_{12} L} \end{bmatrix} \tag{43}$$

Similarly, according to boundary condition of force in Eq. (34).The relationship between **F** and **R** can be expressed as:

$$\mathbf{F} = \mathbf{A} \cdot \mathbf{R} \tag{44}$$

The element of matrix **A** is given by

$$\begin{aligned}
&A_{1j} = -A_3\beta_{1j}\lambda_j + A_3 \quad A_{2j} = (-A_3\beta_{2j}\lambda_j + A_3)\gamma_j \\
&A_{3j} = A_1\lambda_j\alpha_{ij} - A_2\lambda_j \quad A_{4j} = (A_1\lambda_j\alpha_{ij} - A_2\lambda_j)\gamma_j \\
&A_{5j} = A_1\lambda_j - A_0\lambda_j\alpha_{ij} \quad A_{6j} = (A_1\lambda_j - A_0\lambda_j\alpha_{ij})\gamma_j \\
&A_{7j} = -(-A_3\beta_{1j}\lambda_j + A_3)e^{\lambda_j L} \quad A_{8j} = -(-A_3\beta_{2j}\lambda_j + A_3)\gamma_j e^{\lambda_j L} \\
&A_{9j} = -(A_1\lambda_j\alpha_{ij} - A_2\lambda_j)e^{\lambda_j L} \quad A_{10j} = -(A_1\lambda_j\alpha_{ij} - A_2\lambda_j)\gamma_j e^{\lambda_j L} \\
&A_{11j} = -(A_1\lambda_j - A_0\lambda_j\alpha_{ij})e^{\lambda_j L} \quad A_{12j} = -(A_1\lambda_j - A_0\lambda_j\alpha_{ij})\gamma_j e^{\lambda_j L} (j = 1,2,\ldots,12)
\end{aligned} \tag{45}$$

According to Eq. (44) and Eq. (38), the relationship between force vector **F** and displacement vector **d** can be derived as:

$$\mathbf{F} = \mathbf{K} \cdot \mathbf{d} \tag{46}$$

where **K** is dynamic stiffness matrix of two-beam system and can be expressed as:

$$\mathbf{K} = \mathbf{A} \cdot \mathbf{B}^{-1} \tag{47}$$

It is clear that the dynamic stiffness matrix **K** is frequency dependent. The formation method of the global dynamic stiffness matrix which can be obtained through assembling element dynamic stiffness matrix is similar to the finite element method. To compute the frequencies and mode shapes of the two-beam system, the well-established algorithm of Wittrick-Williams need to be applied.

2.3. Dynamic stiffness formulation using precise integration method

Formation of dynamic stiffness matrix in 2.2 section is an exact method. However, stiffness matrix can also be obtained in a more convenient method using precise integration method. According to Eq. (22), **v** can be computed as following:

$$\mathbf{v}(y) = e^{\mathbf{A}y}\mathbf{v}(0) \tag{48}$$

Although above form is concise, precise and efficient computation of matrix exponent is difficult. Matrix exponent can be computed by precise integration method, while computational stability cannot be guaranteed, especially for special kind of matrices. This method may lead to inaccurate results or error results. Recently, Tan and Wu [62] proposed an efficient method to compute matrix exponent, which combines PIM and Pade approximation. The procedure of computing the exponential matrix can be given as follows.

$$\mathbf{T} = \exp(\mathbf{A}y) = \mathbf{I} + \mathbf{T}_a \tag{49}$$

where

$$\mathbf{T}_a = [\mathbf{I} + \mathbf{D}'_{pq}(\mathbf{A}y)]^{-1}[\mathbf{N}'_{pq}(\mathbf{A}y) - \mathbf{D}'_{pq}(\mathbf{A}y)] \tag{50}$$

$$\begin{aligned}
\mathbf{D}'_{pq}(\mathbf{A}y) &= \sum_{j=1}^{q} \frac{(p+q-j)!q!}{(p+q)!j!(q-j)!}(-\mathbf{A}y)^j \\
\mathbf{N}'_{pq}(\mathbf{A}y) &= \sum_{j=1}^{p} \frac{(p+q-j)!p!}{(p+q)!j!(p-j)!}(\mathbf{A}y)^j
\end{aligned} \tag{51}$$

T can be computed using PIM as follows.

$$\mathbf{T}_{a1} = \mathbf{I} + \left[\mathbf{I} + \mathbf{D}'_{pq}\left(\frac{y}{2^N}\mathbf{H}\right)\right]^{-1}\left[\mathbf{N}'_{pq}\left(\frac{y}{2^N}\mathbf{A}\right) - \mathbf{D}'_{pq}\left(\frac{y}{2^N}\mathbf{H}\right)\right] \tag{52}$$

$$\mathbf{T}_{a(i+1)} = 2\mathbf{T}_{ai} + \mathbf{T}_{ai} \times \mathbf{T}_{ai} (i = 1,2,\ldots,N-1) \tag{53}$$

$$\mathbf{T} = \mathbf{I} + \mathbf{T}_{a(N+1)} \tag{54}$$

The computational accuracy of PIM can be determined by parameters p, q and N. These parameters can be determined by adaptive algorithms of selecting parameters [54]. Eq. (48) can also be expressed as:

$$\begin{bmatrix} \mathbf{X} \\ -\mathbf{F_R} \end{bmatrix} = \begin{bmatrix} \mathbf{T}_{11} & \mathbf{T}_{12} \\ \mathbf{T}_{21} & \mathbf{T}_{22} \end{bmatrix} \begin{bmatrix} \mathbf{X_L} \\ \mathbf{F_L} \end{bmatrix} \tag{55}$$

where $\mathbf{X}_R, \mathbf{F}_R$ are the state vectors of the displacement and force at the right end of the element and $\mathbf{X}_L, \mathbf{F}_L$ are the vectors at the left end of the element. After transformation, Eq. (55) can take the following form,

$$\begin{bmatrix} \mathbf{F}_L \\ \mathbf{F}_R \end{bmatrix} = \begin{bmatrix} \mathbf{K}_{11} & \mathbf{K}_{12} \\ \mathbf{K}_{21} & \mathbf{K}_{22} \end{bmatrix} \begin{bmatrix} \mathbf{X}_L \\ \mathbf{X}_R \end{bmatrix} \tag{56}$$

where

$$\begin{aligned}
&\mathbf{K}_{11} = -\mathbf{T}_{12}^{-1} \cdot \mathbf{T}_{11}, \mathbf{K}_{12} = \mathbf{T}_{12}^{-1}, \mathbf{K}_{21} = \mathbf{T}_{21} + \mathbf{T}_{22}\mathbf{T}_{12}^{-1}\mathbf{T}_{11} \\
&\mathbf{K}_{22} = -\mathbf{T}_{22}\mathbf{T}_{22}^{-1}
\end{aligned} \tag{57}$$

Therefore, dynamic stiffness matrix can be obtained by Eq. (57). Although this is a numerical method, results are close to exact solutions if appropriate parameters are selected.

2.4. Winkler layer between two beams with viscous damping

When the viscous damping of the Winkler layer between two beams is taken into consideration, the motion differential equations can also be obtained:

$$-I_0\ddot{v}_1 + A_0 v''_1 + I_1\ddot{\phi}_1 - A_1\phi''_1 = 0 \tag{58}$$

$$-I_0\ddot{w}_1 + A_3 w''_1 - A_3\phi'_1 - K(w_1 - w_2) - Nw''_1 - c(\dot{w}_1 - \dot{w}_2) = 0 \tag{59}$$

$$I_1\ddot{v}_1 - A_1 v''_1 + A_3 w'_1 - I_2\ddot{\phi}_1 + A_2\phi''_1 - A_3\phi_1 = 0 \tag{60}$$

$$-I_0\ddot{v}_2 + A_0 v''_2 + I_1\ddot{\phi}_2 - A_1\phi''_2 = 0 \tag{61}$$

$$-I_0\ddot{w}_2 + A_3 w''_2 - A_3\phi'_2 + K(w_1 - w_2) - Nw''_2 + (K_s w''_2 - K_w w_2) \cdot b + c(\dot{w}_1 - \dot{w}_2) = 0 \tag{62}$$

$$I_1\ddot{v}_1 - A_1 v''_1 + A_3 w'_1 - I_2\ddot{\phi}_1 + A_2\phi''_1 - A_3\phi_1 = 0 \tag{63}$$

where c is a viscous damping factor per unit length. The dynamic stiffness of the two-beam system can be obtained through replacing the stiffness K with the complex stiffness $K + ic\omega$.

2.5. Frequency response function of two-beam system

The frequency response function matrix $\mathbf{H}(\omega)$ of two-beam system can be obtained by inverse of global dynamic stiffness matrix $\mathbf{D}(\omega)$:

$$[\mathbf{H}(\omega)] = [\mathbf{D}(\omega)]^{-1} \tag{64}$$

2.6. Boundary conditions of two-beam system

Boundary conditions of two-beam can be derived by Eq. (13). In this paper, the boundary conditions of hinged-hinged, clamped-hinged, clamped-clamped, clamped-free are considered. For different conditions, the force and displacement of two-beam system should satisfy:

Clamped : $V_1 = W_1 = \Phi_1 = V_2 = W_2 = \Phi_2 = 0$

$$\text{Hinged}: \ V_1 = W_1 = M_1 = V_2 = W_2 = M_2 = 0 \tag{65}$$

$$\text{Free}: \ F_1 = S_1 + N\frac{\partial W_1}{\partial y} = M_1 = 0; F_2 = S_2 + N\frac{\partial W_2}{\partial y} = M_2 = 0$$

2.7. Application of the Wittrick-William algorithm [59]

For free vibration, after applying boundary conditions, the global dynamic stiffness matrix $\mathbf{K}(\omega)$ needs to satisfy [59]:

$$\mathbf{K}(\omega)\mathbf{d} = \mathbf{0} \tag{66}$$

where $\mathbf{d}$ is modal shape vector. In order to obtain the natural frequency of the structure, the dynamic stiffness matrix $\mathbf{K}(\omega)$ should satisfy:

$$|\mathbf{K}(\omega)| = \mathbf{0} \tag{67}$$

Wittrick-William algorithm (W-W) is an efficient algorithm for solving Eq. (54). This algorithm does not directly compute the natural frequency of the structure. In fact, this method is a counting algorithm. According to Wittrick-William algorithm, the number of frequencies which are lower than the given value ω^* can be given by

$$J(\omega^*) = J_0(\omega^*) + s\{\mathbf{K}(\omega^*)\} \tag{68}$$

where $J_0(\omega^*)$ is the total number of frequencies of individual element with fixed boundary conditions which are lower than the given value ω^*. $s\{\mathbf{K}(\omega^*)\}$ is the number of negative elements on the leading diagonal of $\mathbf{K}^{\Delta}$; $\mathbf{K}^{\Delta}$ is the upper triangular matrix which can be obtained through the Gauss elimination method, and $J, J_0, s\{\mathbf{K}(\omega^*)\}$ are integers. The number of natural frequencies in any frequency range can be obtained by Wittrick-William algorithm. The dichotomy is the simplest way to solve the structural frequency. However the computational efficiency of the dichotomy is low. Recently, Yuan Si [60] have proposed a new method named Second order mode-finding method to compute the frequencies and mode shapes efficiently. Due to the limited space of the article, the detailed computational procedure can be found in the literature [60].

2.8. Buckling analysis of two-beam system

For the buckling analysis of two-beam system, the governing equations of two-beam system can be obtained through setting the inertia term to zero in Eqs. (14)–(19). Thus,

$$A_0 v_1'' - A_1 \phi_1'' = 0 \tag{69}$$

$$A_3 w_1'' - A_3 \phi_1' - K(w_1 - w_2) - N w_1'' = 0 \tag{70}$$

$$-A_1 v_1'' + A_3 w_1' + A_2 \phi_1'' - A_3 \phi_1 = 0 \tag{71}$$

$$A_0 v_2'' - A_1 \phi_2'' = 0 \tag{72}$$

$$A_3 w_2'' - A_3 \phi_2' + K(w_1 - w_2) - N w_2'' + (K_s w_2'' - K_w w_2) \cdot b = 0 \tag{73}$$

$$-A_1 v_1'' + A_3 w_1' + A_2 \phi_1'' - A_3 \phi_1 = 0 \tag{74}$$

The static stiffness matrix $\mathbf{K}(N)$ of the two-beam system under the axial forces is obtained by setting the frequency term ω^2 to zero in dynamic stiffness matrix. Similarly, the global stiffness matrix can be assembled by element stiffness matrix. By applying boundary conditions, which is similar to the finite element method, global stiffness matrix $\mathbf{K}(N)$ should satisfy [59]:

$$\mathbf{K}(N)\mathbf{d} = \mathbf{0} \tag{75}$$

where $\mathbf{d}$ is the displacement vector. To obtain the buckling load N of the double-beam system, the stiffness matrix $\mathbf{K}(N)$ should satisfy:

$$|\mathbf{K}(N)| = 0 \tag{76}$$

It is clear that the lowest positive solution of Eq. (76) is the critical buckling load of the two-beam system, and Eq. (76) can also be solved by the Wittrick-William algorithm mentioned in 2.7.

2.9. Dynamic characteristics of double beam system under moving load

In this section, we analyze the dynamic characteristics of double functionally graded beam system under moving load. The standard linear solid model [35] is applied to simulate the dynamic behavior of the viscoelastic inner layer, which is made of Maxwell's element and elastic spring as shown in Fig. 4. According to literature [35], the complex-valued stiffness between two layers can be expressed as:

$$k_{inn}(\omega) = K_0 + K_1 \frac{i\tau\omega}{1 + i\tau\omega} \tag{77}$$

where $i = \sqrt{-1}$ is the imaginary unit and τ is the relaxation time of the viscoelastic material. The relationship between force and displacement can be obtained as [35]:

$$F_{inn} = \hat{K}_{inn} * \dot{d}_r(t) = \int_{-\infty}^{t} \hat{K}_{inn}(t-s)\dot{d}_r(s)ds \tag{78}$$

where $*$ denotes the convolution operator, the over-dot represents derivative with respect to time t. $d_r(t)$ is the pertinent displacement. $\hat{K}_{inn}(t)$ is the relaxation function and can be derived as,

$$\hat{K}_{inn}(t) = F^{-1}\left(\frac{1}{i\omega}k_{inn}(\omega)\right) \tag{79}$$

where F^{-1} represents inverse Fourier transform. The moving load on the upper beam can be expressed as follows

$$F(x,t) = f \cdot e^{i\Omega t}\delta(x - vt) \tag{80}$$

where f is moving force amplitude and δ represents dirac function. Ω and v are harmonic excitation frequency and moving speed. External force potential energy can be expressed as:

$$U_{ext} = -\int_0^L F(x,t) \cdot w_1(x,t)dx \tag{81}$$

Using Hamilton's principle, we can obtain

$$\delta \int_{t_1}^{t_2} (T - U - U_{ext})dt = 0 \tag{82}$$

Through the symbolic operation, Eq. (82) can be written as following:

$$-I_0 \ddot{v}_1 + A_0 v_1'' + I_1 \ddot{\phi}_1 - A_1 \phi_1'' = 0 \tag{83}$$

$$-I_0 \ddot{w}_1 + A_3 w_1'' - A_3 \phi_1' - \hat{K}_{inn}(t) * (\dot{w}_1 - \dot{w}_2) - N w_1'' + F(x,t) = 0 \tag{84}$$

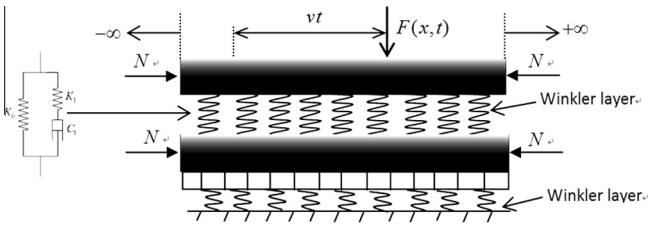

Fig. 4. The double beam system under moving load.

$$I_1\ddot{v}_1 - A_1v_1'' + A_3w_1' - I_2\phi_1'' + A_2\phi_1'' - A_3\phi_1 = 0 \tag{85}$$

$$-I_0\ddot{v}_2 + A_0v_2'' + I_1\ddot{\phi}_2 - A_1\phi_2'' = 0 \tag{86}$$

$$-I_0\ddot{w}_2 + A_3w_2'' - A_3\phi_2' + \hat{K}_{inn}(t) * (\dot{w}_1 - \dot{w}_2) - Nw_2'' + (K_sw_2'' - K_ww_2)\cdot b = 0 \tag{87}$$

$$I_1\ddot{v}_2 - A_1v_2'' + A_3w_2' - I_2\phi_2'' + A_2\phi_2'' - A_3\phi_2 = 0 \tag{88}$$

where * denotes the convolution operator. Transforming above equations from the time domain t to the frequency ω, we can obtain

$$\frac{\partial \mathbf{v}}{\partial x} = \bar{\mathbf{A}}\cdot\mathbf{v} + \mathbf{F} \tag{89}$$

where $\mathbf{F} = [0,0,0,F(x,\omega),0,0,0,0,0,0,0,0]^T$ and $\mathbf{v} = [W_1,\Phi_1,V_1,S_1,M_1,F_1,W_2,\Phi_2,V_2,S_2,M_2,F_2]^T$. For example, $W_1(x,\omega)$ can be transformed from $w_1(x,t)$ using Fourier transform. $\bar{\mathbf{A}}$ can be obtained from Eq. (22) by replacing variable K with $k_{inn}(\omega)$. After transformation from the space-frequency domain (x,ω) to the wavenumber-frequency (ξ,ω), Eq. (75) can be transformed into such form

$$i\xi\cdot\mathbf{E}\cdot\bar{\mathbf{v}} = \bar{\mathbf{A}}(\xi,\omega)\cdot\bar{\mathbf{v}} + \bar{\mathbf{F}}(\xi,\omega) \tag{90}$$

where $\bar{\mathbf{F}}(\xi,\omega) = [0,0,0,4\pi^2\delta(\omega+\xi v-\Omega),0,0,0,0,0,0,0,0]^T$. $\mathbf{E}$ is 12×12 unit matrix, Eq. (90) can also be written as

$$(i\xi\cdot\mathbf{E} - \bar{\mathbf{A}}(\xi,\omega))\cdot\bar{\mathbf{v}} = \bar{\mathbf{F}}(\xi,\omega) \tag{91}$$

where i is $\sqrt{-1}$. Solving for $\mathbf{v}$ from above equation

$$\bar{\mathbf{v}} = (i\xi\cdot\mathbf{E} - \bar{\mathbf{A}}(\xi,\omega))^{-1}\bar{\mathbf{F}}(\xi,\omega) \tag{92}$$

Therefore, $\tilde{\mathbf{v}}$ can be computed through transforming above equation from wavenumber-frequency to wavenumber-time,

$$\tilde{\mathbf{v}} = (i\xi\cdot\mathbf{E} - \bar{\mathbf{A}}(\xi,\omega=\Omega-\xi v))^{-1}\tilde{\mathbf{F}} \tag{93}$$

where $\tilde{\mathbf{F}} = (0,0,0,2\pi\cdot e^{i(\Omega-\xi v)t},0,0,0,0,0,0,0,0)^T$. Thus, $\mathbf{v}$ can be derived using Fourier transformation from wavenumber-time domain to space-time domain

$$\mathbf{v} = \frac{1}{2\pi}\int_{-\infty}^{+\infty}\tilde{\mathbf{v}}\cdot e^{i\xi x}d\xi \tag{94}$$

Equation above can be solved using fast discrete Fourier inverse transform. For example,

$$v(x,t) = \frac{1}{2\pi}\int_{-\infty}^{+\infty}V(\xi,t)d\xi \approx \frac{\Delta\xi}{2\pi}\sum_{j=-N+1}^{N}W(\xi_j,t)e^{i\xi_jx} \tag{95}$$

where

$$\xi_k = (k-N)\Delta\xi - \frac{\Delta\xi}{2},\quad k = 1,2,\ldots,2N \tag{96}$$

Substituting Eq. (96) into Eq. (95),

$$v(x_m,t) \approx \frac{\Delta\xi}{2\pi}\sum_{k=1}^{2N}V(\xi_k,t)e^{i\xi_kx_m} \tag{97}$$

where

$$x_m = (m-N)\Delta x, m = 1,2,\cdots,2N \tag{98}$$

and

$$\Delta x\cdot\Delta\xi = \frac{\pi}{N} \tag{99}$$

Thus,

$$\Delta x = \frac{\pi}{N\Delta\xi} \tag{100}$$

$$\xi_kx_m = -\left(N-\frac{1}{2}\right)(m-N)\frac{\pi}{N} + (k-1)(m-N)\frac{\pi}{N} \tag{101}$$

Using Eq. (101) and Eq. (97), $v(x_m,t)$ can expressed as following:

$$v(x_m,t) \approx \frac{\Delta\beta}{2\pi}e^{-i(N-\frac{1}{2})(m-N)\pi/N}\sum_{k=1}^{2N}V(\xi_k,t)e^{i(k-1)(m-N)\pi/N} \tag{102}$$

Eq. (94) can be computed following above procedure. We need to mention that the number of sampling points should be large enough to obtain accurate results. To aviod aliasing, sampling frequency $2\pi/\Delta\xi$ should satisfy Nyquist criterion [53]. However, when moving speed increases, sampling frequency must increase to aviod aliasing. Therefore, convergence of results should be tested.

2.10. Interval analysis of double beam system under moving load with uncertain-but-bounded parameters

To analyze dynamic response of double beam system under moving load with uncertain parameters, Eq. (93) can be rewritten as:

$$\mathbf{Z}\cdot\mathbf{v} = \mathbf{F} \tag{103}$$

where $\mathbf{Z}$ can be expressed as

$$\mathbf{Z} = i\xi\cdot\mathbf{E} - \bar{\mathbf{A}}(\xi,\omega=\Omega-\xi v) \tag{104}$$

Assume that parameters of beam system are uncertain-but-bounded vector $\mathbf{a}$, which can be expressed as:

$$\mathbf{a}_I = [\mathbf{a}_{lower},\mathbf{a}_{upper}] \tag{105}$$

where $\mathbf{a}_{lower}$ and $\mathbf{a}_{upper}$ represent the lower and upper bounds of the uncertain parameter vector $\mathbf{a}$. $\mathbf{Z}$ and $\mathbf{v}$ are complex matrix and complex vector respectively. Thus, Eq. (103) can be rewritten as:

$$(\mathbf{Z}_{real} + i\cdot\mathbf{Z}_{imag})\cdot(\mathbf{v}_{real} + i\cdot\mathbf{v}_{imag}) = \mathbf{F}_{real} + i\cdot\mathbf{F}_{imag} \tag{106}$$

The above equation can be expressed as:

$$\begin{bmatrix}\mathbf{Z}_{real} & -\mathbf{Z}_{imag}\\ -\mathbf{Z}_{imag} & \mathbf{Z}_{real}\end{bmatrix}\begin{bmatrix}\mathbf{v}_{real}\\ \mathbf{v}_{imag}\end{bmatrix} = \begin{bmatrix}\mathbf{F}_{real}\\ \mathbf{F}_{imag}\end{bmatrix} \tag{107}$$

With the interval extension, Eq. (107) can be rewritten as:

$$\hat{\mathbf{Z}}(\mathbf{a}_I)\hat{\mathbf{v}}_I = \hat{\mathbf{F}} \tag{108}$$

where $\hat{\mathbf{v}}_I$ is the theoretical solution set, which can be expressed as:

$$\hat{\mathbf{v}}_I = [\hat{\mathbf{v}}_l,\hat{\mathbf{v}}_u] \tag{109}$$

To solve Eq. (108), interval matrix $\hat{\mathbf{Z}}(\mathbf{a}_I)$ can be approximated by using Taylor series expansion:

$$\mathbf{Z}(\mathbf{a}_I) = \mathbf{Z}(\mathbf{a}_m) + \sum_{i=1}^{k}\Delta a_{Ii}\frac{\partial\mathbf{Z}(\mathbf{a}_m)}{\partial a_i} = \mathbf{Z}_m + \Delta\mathbf{Z}_I \tag{110}$$

where $\mathbf{a}_m$ is the interval mean value of the interval vector $\mathbf{a}_I$. a_{Ii} represents interval parameter $a_i(i=1\cdots k)$. Δa_{Ii} can be expressed as:

$$\Delta a_{Ii} = [-\Delta a_i,\Delta a_i] \tag{111}$$

Therefore, we can obtain:

$$\mathbf{a}_m = (\mathbf{a}_{lower} + \mathbf{a}_{upper})/2\Delta\mathbf{a} = (\mathbf{a}_{upper} - \mathbf{a}_{lower})/2 \tag{112}$$

Inserting Eq. (110) into Eq. (108),

$$(\hat{\mathbf{Z}}_m + \Delta\hat{\mathbf{Z}}_I)\cdot(\hat{\mathbf{v}}_m + \Delta\hat{\mathbf{v}}_I) = \hat{\mathbf{F}} \tag{113}$$

Thus,

$$\hat{\mathbf{v}}_m + \Delta\hat{\mathbf{v}}_I = (\hat{\mathbf{Z}}_m + \Delta\hat{\mathbf{Z}}_I)^{-1}\hat{\mathbf{F}} \tag{114}$$

Table 1
Comparison of frequencies (rad/s) under the S-S boundary condition.

K (N/m)	1 (Present)	1 (Ref)	2 (Present)	2 (Ref)	3 (Present)	3 (Ref)
1×10^5	48.8632	48.9	90.6621	90.7	183.1910	183.2
2×10^5	66.2746	66.3	101.2112	101.2	188.6054	188.6
3×10^5	79.1256	79.9	110.6031	110.6	193.7911	193.8

If the spectral radius of matrix $(\mathbf{Z}_m)^{-1}\Delta\mathbf{Z}$ is less than 1, equation above can be rewritten as follows using Neumann series:

$$\hat{\mathbf{v}}_m + \Delta\hat{\mathbf{v}}_I = (\hat{\mathbf{Z}}_m)^{-1}\hat{\mathbf{F}} + \sum_{\gamma=1}^{\infty}(\hat{\mathbf{Z}}_m)^{-1}(-\Delta\mathbf{Z}_I(\mathbf{Z}_m)^{-1})^{\gamma}\hat{\mathbf{F}} \tag{115}$$

Ignoring the higher order terms, the equation above can be simplified as follows:

$$\hat{\mathbf{v}}_m = (\mathbf{Z}_m)^{-1}\hat{\mathbf{F}} \tag{116}$$

$$\Delta\hat{\mathbf{v}}_I = -(\hat{\mathbf{Z}}_m)^{-1}\Delta\mathbf{Z}_I\hat{\mathbf{v}}_m \tag{117}$$

Substituting Eq. (110) into Eq. (117), we can obtain:

$$\Delta\hat{\mathbf{v}}_I = -(\hat{\mathbf{Z}}_m)^{-1}\left(\sum_{i=1}^{k}\Delta a_{Ii}\frac{\partial\mathbf{Z}(\mathbf{a}_m)}{\partial a_i}\right)\hat{\mathbf{v}}_m \tag{118}$$

It is clear that $\Delta\hat{\mathbf{v}}_I$ is a monotonic function with respect to Δa_{Ii}. Therefore, the lower and upper bounds can be expressed as:

$$\hat{\mathbf{v}}_{lower} = \hat{\mathbf{v}}_m - \left|(\hat{\mathbf{Z}}_m)^{-1}\left(\sum_{i=1}^{k}\Delta a_{Ii}\left|\frac{\partial\mathbf{Z}(\mathbf{a}_m)}{\partial a_i}\hat{\mathbf{v}}_m\right|\right)\right| \tag{119}$$

$$\hat{\mathbf{v}}_{upper} = \hat{\mathbf{v}}_m + \left|(\hat{\mathbf{Z}}_m)^{-1}\left(\sum_{i=1}^{k}\Delta a_{Ii}\left|\frac{\partial\mathbf{Z}(\mathbf{a}_m)}{\partial a_i}\hat{\mathbf{v}}_m\right|\right)\right| \tag{120}$$

where $|\cdot|$ represents the absolute value. The interval of $v(x,t)$ can be obtained through Eq. (102).The derivative of matrix $\mathbf{Z}$ with respect to a_i can be expressed as:

$$\frac{\partial\mathbf{Z}(\mathbf{a}_m)}{\partial a_i} = -\frac{\partial\bar{\mathbf{A}}(\mathbf{a}_m)}{\partial a_i} \tag{121}$$

3. Numerical results and discussion

To verify the correctness of the results in this paper, numerical results of free vibration of simply supported beams are compared with literature [27]. In literature [27], the material of two-beam system is homogeneous. The values of parameters are: $E = 1\times10^{10}$ N/m^2, $A = 5\times10^{-2}$, $I = 4\times10^{-4}$, $L = 10$ m, $\rho = 2\times10^3$ kg/m^3, $K_s = K_w = 0$, where A and I are area and moment of inertia. The results of first three natural frequencies are compared in table 1. From table 1, it is observed that the present numerical results are in good agreement with literature [27].

To analyze the buckling and dynamic characteristics of two-functionally graded Timoshenko beam system, the geometrical properties of two-beam system are as follows: $b = 0.1$ m,$h = 0.1$ m. The material properties of metal are: $E_m = 70$ Gpa, $v_m = 0.23$, $\rho_m = 2700$ kg/m^3. The material properties of ceramic are: $E_c = 380$ Gpa, $v_c = 0.23$ Gpa, $\rho_c = 3800$ kg/m^3 and shear coefficient $\kappa = 5/6$.

3.1. Vibration analysis of two-beam system

The non-dimensional natural frequency of the two-beam system can be defined as:

$$\lambda = \frac{\omega L_0^2}{h_0}\sqrt{\rho_m/E_m} \tag{122}$$

where L_0 and h_0 are constants as follows:

$$L_0 = 1m, \quad h_0 = 0.1m$$

The effects of the slenderness ratio L/h and gradient parameter k on the fundamental non-dimensional natural frequency of two-beam system are showed in Tables 2–5. The stiffness of Winkler elastic layer between two beams is $K = 10^5$ N/m and the axial force $N = 0$. The parameters of the foundation are $K_s = K_w = 0$. According to Tables 2–5, for different slenderness ratio $L/h(L = 1$ m), the fundamental frequency decreases with the increase of gradient parameter k under different boundary conditions. It is noticeable that increase of gradient parameter k can both increase the bending stiffness and the mass of the two-beam system, while the effect of the mass increase is more significant compared to bending stiffness, and the boundary condition has great influence on the fundamental frequency. The slenderness ratio obviously affects non-dimensional natural frequency as shown in Tables 2–5. In general, with the increase of slenderness ratio, non-dimensional natural frequency decreases rapidly.

It is clear that the Winkler layer between the two beams greatly affects the frequencies corresponding to reverse modes of double beam, but have little effect on other forms of vibration modes. Fig. 5 shows the influence of the stiffness K of connecting layer on the fundamental frequency of two-beam system under different boundary conditions. The length of two-beam system is $L = 5$ m. Parameters of the foundation are $K_s = K_w = 0.01$ Gpa and the axial force $N = 0$. The other parameters are the same as before. It is seen that the increase of the stiffness of the connecting layer can increase the fundamental frequency under different boundary conditions. C, F, H denote clamped, free and hinged.

Fig. 4 plots the effect of elastic foundation parameters K_w, K_s on the non-dimensionless fundamental frequency$\lambda$of the two-beam system under the boundary condition C—C and H—H. The length of two-beam system is $L = 5$ m and gradient parameter $k = 1$. The stiffness of elastic layer is $K = 10^5$ N/mand the axial force is $N = 0$. The range of K_w, K_s is 0.01–0.1 Gpa. It is clear that with

Table 2
The fundamental non-dimensional natural frequency λ of two-beam system under CC boundary conditions.

L/h	$k=0.1$	$k=0.2$	$k=0.5$	$k=1$	$k=2$	$k=5$	$k=10$
10	11.4911	11.1001	10.1613	9.1798	8.3394	7.8333	7.5356
20	6.0066	5.7966	5.2946	4.7751	4.3412	4.1064	3.9697
50	2.4398	2.3543	2.1503	1.9399	1.7660	1.6757	1.6233
100	1.2609	1.2203	1.1238	1.0257	0.9465	0.9082	0.8858

Table 3
The fundamental non-dimensional natural frequencies λ of two-beam system under HH boundary conditions.

L/h	$k=0.1$	$k=0.2$	$k=0.5$	$k=1$	$k=2$	$k=5$	$k=10$
10	5.3099	5.1475	4.8066	4.5049	4.2530	3.9723	3.6978
20	2.6867	2.6043	2.4315	2.2796	2.1541	2.0155	1.8774
50	1.0899	1.0574	0.9896	0.9304	0.8822	0.8292	0.7759
100	0.6259	0.6133	0.5878	0.5667	0.5509	0.5349	0.5167

Table 4
The fundamental non-dimensional natural frequencies λ of two-beam system under CH boundary conditions.

L/h	$k=0.1$	$k=0.2$	$k=0.5$	$k=1$	$k=2$	$k=5$	$k=10$
10	8.1161	7.8415	7.1961	6.5400	5.9877	5.6316	5.3935
20	4.1681	4.0249	3.6895	3.3509	3.0704	2.8998	2.7846
50	1.6877	1.6302	1.4957	1.3604	1.2494	1.1837	1.1389
100	0.8996	0.8737	0.8139	0.7553	0.7092	0.6847	0.6676

Table 5
The fundamental non-dimensional natural frequencies λ of two-beam system under CF boundary conditions.

L/h	$k=0.1$	$k=0.2$	$k=0.5$	$k=1$	$k=2$	$k=5$	$k=10$
10	1.9040	1.8370	1.6770	1.5118	1.3745	1.3023	1.2605
20	0.9591	0.9257	0.8454	0.7627	0.6943	0.6589	0.6385
50	0.4159	0.4041	0.3766	0.3492	0.3280	0.3190	0.3137
100	0.3632	0.3615	0.3569	0.3514	0.3470	0.3473	0.3463

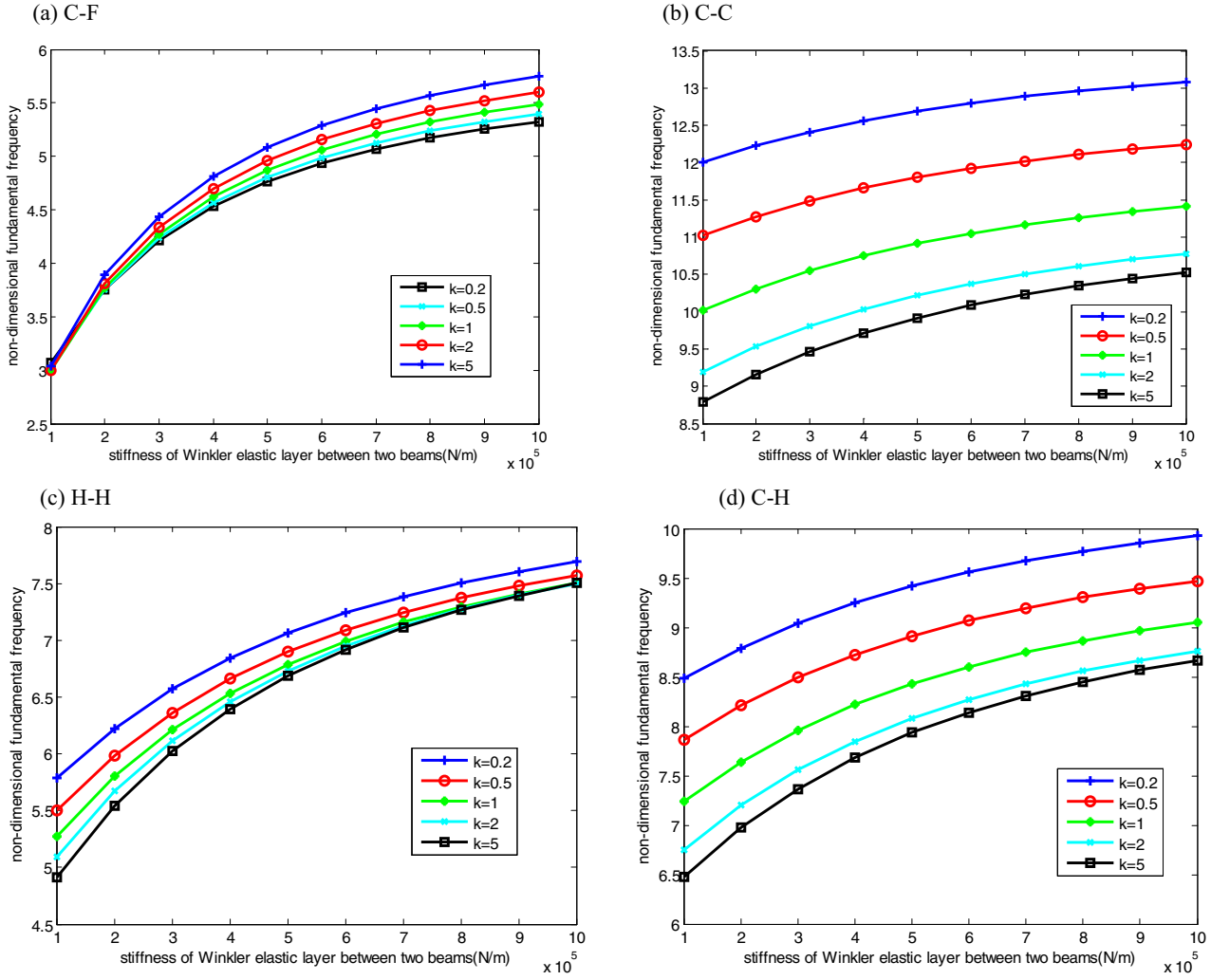

Fig. 5. The influence of the stiffness K on fundamental frequency of two-beam system: (a) clamped-free (b) clamped-clamped(c) hinged-hinged (d) clamped-hinged.

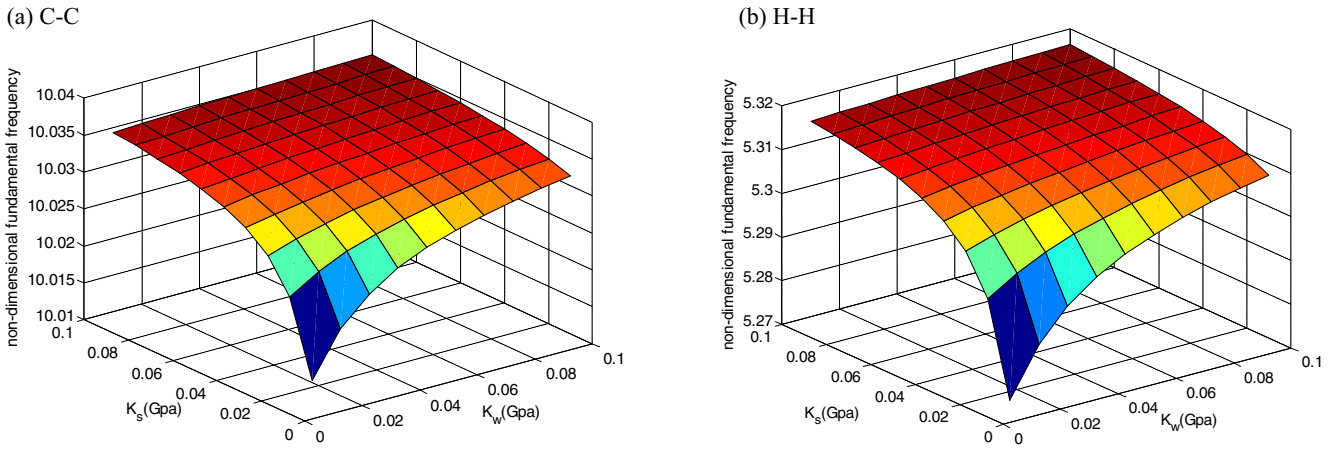

Fig. 6. The influence of the foundation parameters K_w, K_s on fundamental frequency of two-beam system: (a) clamped-clamped (b) simple-simple.

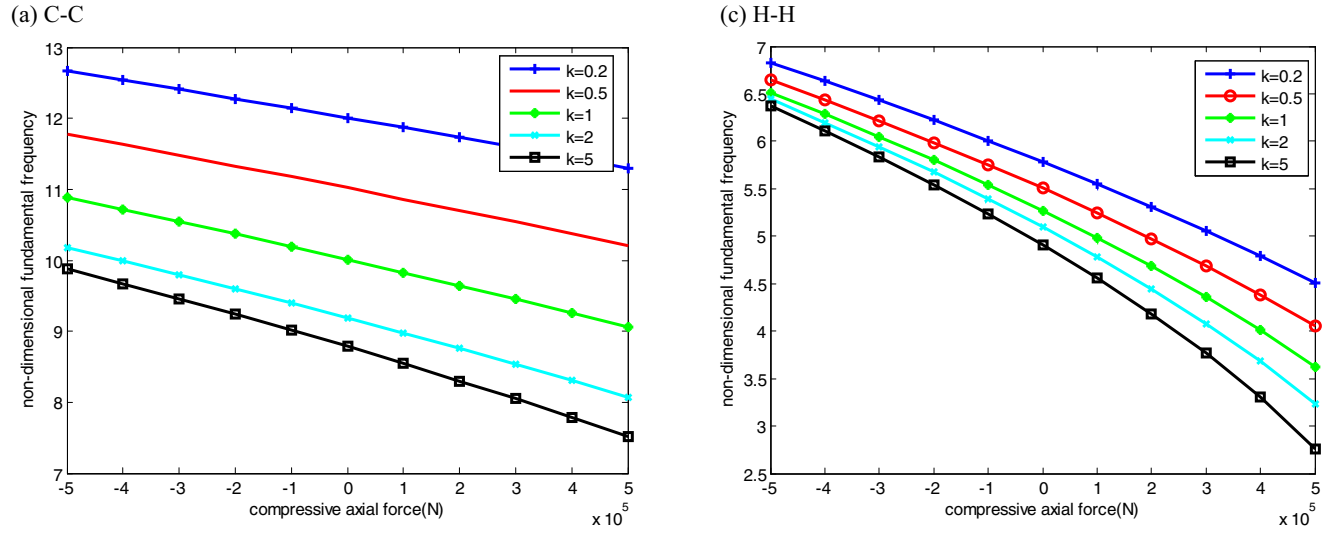

Fig. 7. The influence of the compressive axial force on fundamental frequency of two-beam system: (a) clamped-clamped (b) hinged-hinged.

the increase of the parameter K_w, K_s, the fundamental frequency of the two-beam system will increase, because the increase of the stiffness of the elastic foundation will increase the stiffness of the whole system. However, fundamental frequency keeps almost constant when the values of the K_w, K_s approximate 0.1 Gpa. Fig. 6 shows that the effects of Winkler layer and shear layer on fundamental frequency are close. Fig. 7 plots the effect of compressive axial force on the fundamental frequency of the two-beam system under C—C and H—H boundary conditions. Fig. 7 shows that increasing the compressive axial force lead to the decrease of system stiffness.

Figs. 8 and 9 shows that the effect of viscous damping factor c on the frequency response function of the two-beam system under C—C and H—H boundary conditions, where foundation parameters are $Ks = 0.01$ Gpa,$Kw = 0$, gradient parameter is $k = 1$, and the axial force is $N = 0$. Figs. 8 and 9 show the origin FRF of transverse displacement at position 1 and the cross-point FRF at position 2 under the excitation at position 1 along the z direction. Position 1 and position 2 denote the midpoints of two beams as shown in Fig. 1. It is observed that the damping factor has a significant effect on the second-order frequency, because second-order mode is a reverse mode of two beams and the value of the frequency increase with the increase of the damping factor c. However, for fundamental frequency, the damping factor only affects the peak value of frequency response function. Because the mode shape of fundamental frequency is a similar mode of two beams along the same direction, the damping factor has a little influence on the value of fundamental frequency. It is obvious that the amplitude of the cross-point FRF decreases compared to the origin FRF due to the damping layer between the two beams. Similar mode denotes deflections of two beams towards the same direction, while reverse mode denotes deflections of two beams towards opposite direction as shown below:

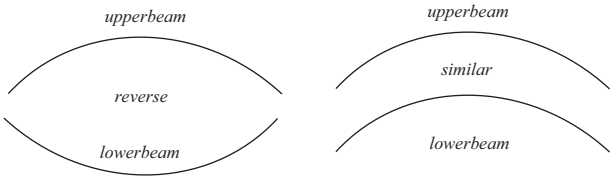

In order to investigate the effect of gradient parameter k on dynamic characteristic of two-beam system with damping, the loss factor η of the system can be defined as [61]

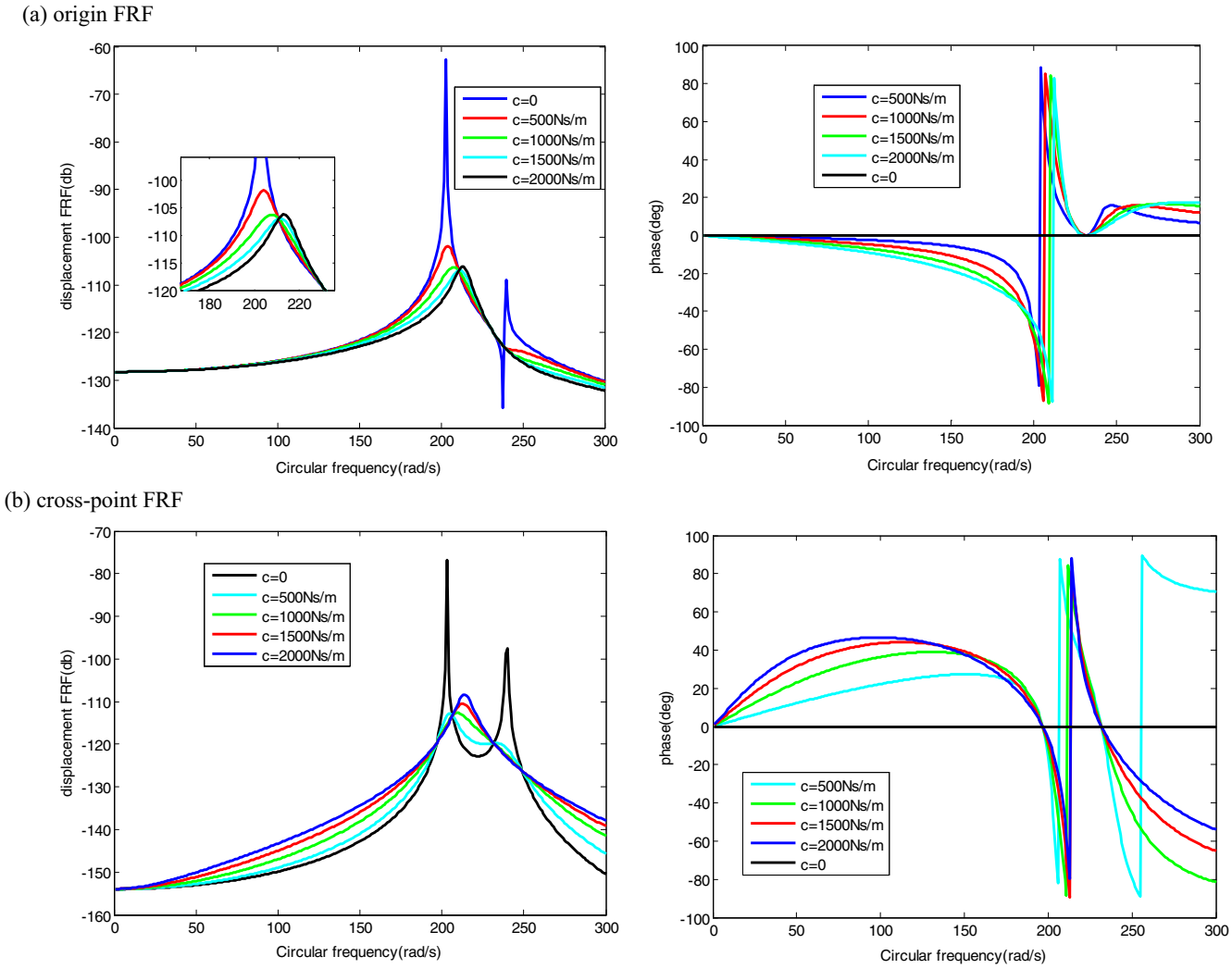

Fig. 8. The influence of the damping factor c on the amplitude and phase of FRF under C—C boundary condition: (a) origin FRF (b) cross-point FRF.

$$\eta = \frac{\mathrm{Im}(\omega_n^2)}{\mathrm{Re}(\omega_n^2)} \tag{123}$$

where ω_n^2 is the nth complex natural frequency. Fig. 10 shows the influence of gradient parameter k on the loss factor η of the system under C—C and H-H boundary conditions. Damping factor c is $10^3 Ns/m$. The stiffness of elastic layer is $K = 10^5$ N/m and foundation parameters are $Ks = 0.01$ Gpa and $Kw = 0$. It can be observed that the increase of gradient parameter k can increase the loss factor of the two-beam system, and the parameters of foundation have great effect on the loss factor.

3.2. Buckling analysis of two-beam system

In this section, numerical results of buckling analysis of two-beam system are analyzed. The length of the beam is $L = 5$ m , the geometrical properties of two-beam system are as follows: $b = 0.1$ m,$h = 0.1$ m. The material properties of metal are: $E_m = 70$ Gpa, $v_m = 0.23$, $\rho_m = 2700$ kg/m^3. The material properties of ceramic are: $E_c = 380$ Gpa, $v_c = 0.23$ Gpa, $\rho_c = 3800$ kg/m^3 and shear coefficient $\kappa = 5/6$. The non-dimensional buckling load can be defined as:

$$p^* = \frac{pL^2}{\pi^2 E_m I} \tag{124}$$

where I is cross sectional moment of inertia.

Tables 6–8 show that the buckling load decreases with the increase of the gradient parameter k under different boundary conditions. It can also be observed that the increase of the connecting stiffness K will increase the buckling load. For different foundation parameters, the effect of stiffness K_s of shear layer on buckling load is similar to the effect of stiffness K_w of Winkler layer according to Tables 6–8.

3.3. Dynamic characteristic analysis of double-beam system under moving load

In this section, the geometry dimensions of double beam system are $b = 0.1$ m,$h = 0.1$ m for both beams. The material properties of metal are $E_m = 70$ Gpa, $v_m = 0.23$ and $\rho_m = 2700$ kg/m^3. Similarly, the material properties of ceramic are $E_c = 380$ Gpa, $v_c = 0.23$ $\rho_c = 3800$ kg/m^3 and shear coefficient $\kappa = 5/6$. Winkler-type equilibrium modulus is $K_0 = 30$ kN/m^2, and Maxwell's parameter is $K_1 = 5K_0$. Relaxation time is $\tau = 0.2$ s for inner layer. The elastic foundation parameters are $K_s = K_w = 0.01$ Gpa. Axial load is $N = 0$. Characteristic parameters of moving load are $f = 1000$ N and $\Omega = 0$. (a) $v = 50$ m/s,$t = 0.1$ s (b) $v = 200$ m/s,$t = 0.1$ s

According to Fig. 11, displacement responses corresponding to different speeds are shown. It is noticeable that the track deflection is close to deformation of the structure under static load, when the speed of moving load is far lower than critical speed. However,

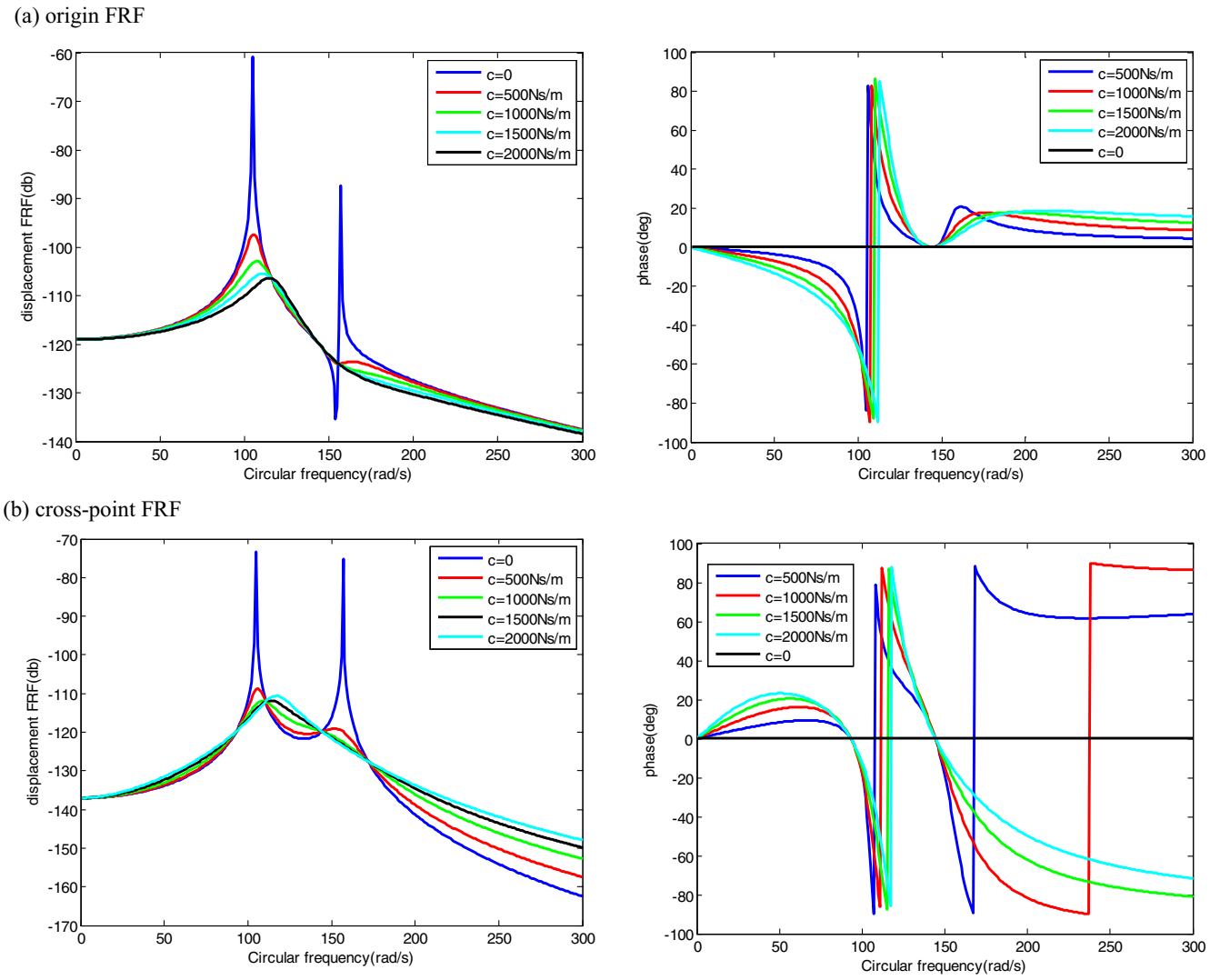

Fig. 9. The influence of the damping factor c on the amplitude and phase of FRF under H-H boundary condition: (a) origin FRF (b) cross-point FRF.

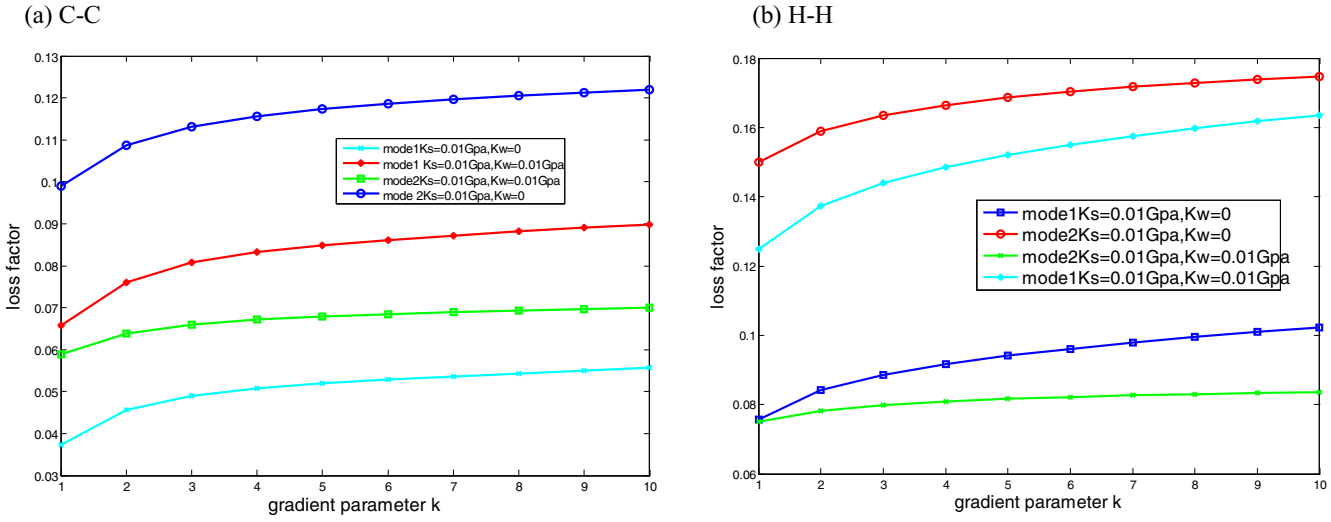

Fig. 10. The influence of the gradient k on the loss factor: (a) clamped-clamped(b) hinged-hinged.

when the speed of load exceeds critical speed, structure begins to vibrate in wide area as shown in Fig. 11(b). In Fig. 11, the dotted line represents lower beam and the solid line denotes upper beam. It is clear that different values of gradient parameter have a significant effect on the deflection of double-beam system. Displacement of upper beam in time domain can be seen in Fig. 12.

Table 6
The non-dimensional buckling load P^* of two-beam system under CC boundary conditions.

	K(N/m)	$k=0.1$	$k=0.2$	$k=0.5$	$k=1$	$k=2$	$k=5$	$k=10$
$K_s=0.01$ $K_w=0$	10^5	20.1663	18.4066	14.6961	11.4558	9.0844	7.7792	7.1408
	2×10^5	20.5832	18.8232	15.1118	11.8703	9.4973	8.1906	7.5519
	3×10^5	20.8407	19.0804	15.3685	12.1260	9.7520	8.4443	7.8043
$K_s=0$ $K_w=0.01$	10^5	20.2364	18.4767	14.7665	11.5264	9.1554	7.8504	7.2121
	2×10^5	20.8207	19.0677	15.3496	12.1083	9.7355	8.4287	7.7892
	3×10^5	21.2735	19.5132	15.8011	12.5582	10.1834	8.8746	8.2338
$K_s=0.01$ $K_w=0.01$	10^5	20.2638	18.5041	14.7938	11.5537	9.1825	7.8773	7.2389
	2×10^5	20.9239	19.1693	15.4525	12.2108	9.8375	8.5299	7.8900
	3×10^5	21.4861	19.7256	16.0128	12.7689	10.3928	9.0825	8.4406

Table 7
The non-dimensional buckling load P^* of two-beam system under HH boundary conditions.

	K(N/m)	$k=0.1$	$k=0.2$	$k=0.5$	$k=1$	$k=2$	$k=5$	$k=10$
$K_s=0.01$ $K_w=0$	10^5	5.7422	5.3401	4.5631	3.3957	3.4467	2.9867	2.6488
	2×10^5	6.1848	5.7836	5.0057	4.3782	3.8890	3.4287	3.0907
	3×10^5	6.4255	6.0243	5.2464	4.6188	4.1296	3.6692	3.3311
$K_s=0$ $K_w=0.01$	10^5	5.8958	5.4946	4.7168	4.0893	3.6000	3.1401	2.8025
	2×10^5	6.6802	6.2790	5.5011	4.8732	4.3832	3.9232	3.5858
	3×10^5	7.2893	6.8881	6.1101	5.4819	4.9913	4.5312	4.1940
$K_s=0.01$ $K_w=0.01$	10^5	5.9261	5.5250	4.7471	4.1196	3.6302	3.1703	2.8326
	2×10^5	6.7941	6.3929	5.6149	4.9859	4.4967	4.0364	3.6988
	3×10^5	7.5226	7.1214	6.3432	5.7148	5.2237	4.7629	4.4232

Table 8
The non-dimensional buckling load P^* of two-beam system under CH boundary conditions.

	K(N/m)	$k=0.1$	$k=0.2$	$k=0.5$	$k=1$	$k=2$	$k=5$	$k=10$
$K_s=0.01$ $K_w=0$	10^5	10.7088	9.8225	7.9808	6.3950	5.2246	4.5019	4.1020
	2×10^5	11.1334	10.2468	8.4041	6.8168	5.6448	4.9203	4.5189
	3×10^5	11.3863	10.4994	8.6560	7.0677	5.8946	5.1691	4.7671
$K_s=0$ $K_w=0.01$	10^5	10.7985	9.9123	8.0712	6.4859	5.3162	4.5934	4.1930
	2×10^5	11.4318	10.5452	8.7031	7.1166	5.9451	5.2187	4.8147
	3×10^5	11.9213	11.0341	9.1905	7.6020	6.4276	5.6970	5.2890
$K_s=0.01$ $K_w=0.01$	10^5	10.8267	9.9405	8.0993	6.5139	5.3440	4.6211	4.2206
	2×10^5	11.5377	10.6510	8.8085	7.2216	6.0495	5.3223	4.9176
	3×10^5	12.1388	11.2513	9.4068	7.8171	6.6412	5.9085	5.4990

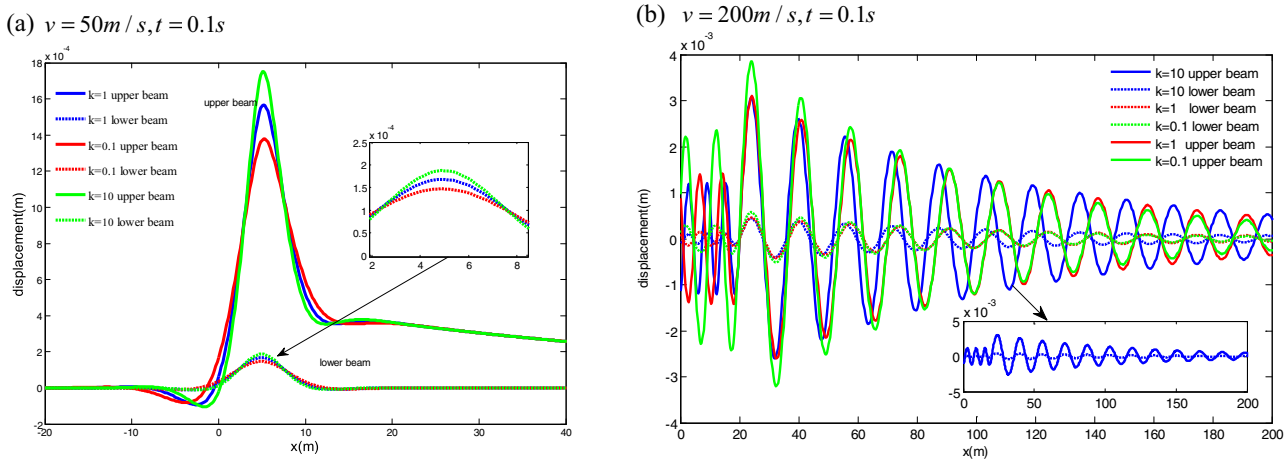

Fig. 11. Displacement response of the double-beam system under moving load: (a) $v=50$ m/s,$t=0.1$ s (b) $v=200$ m/s,$t=0.1$ s.

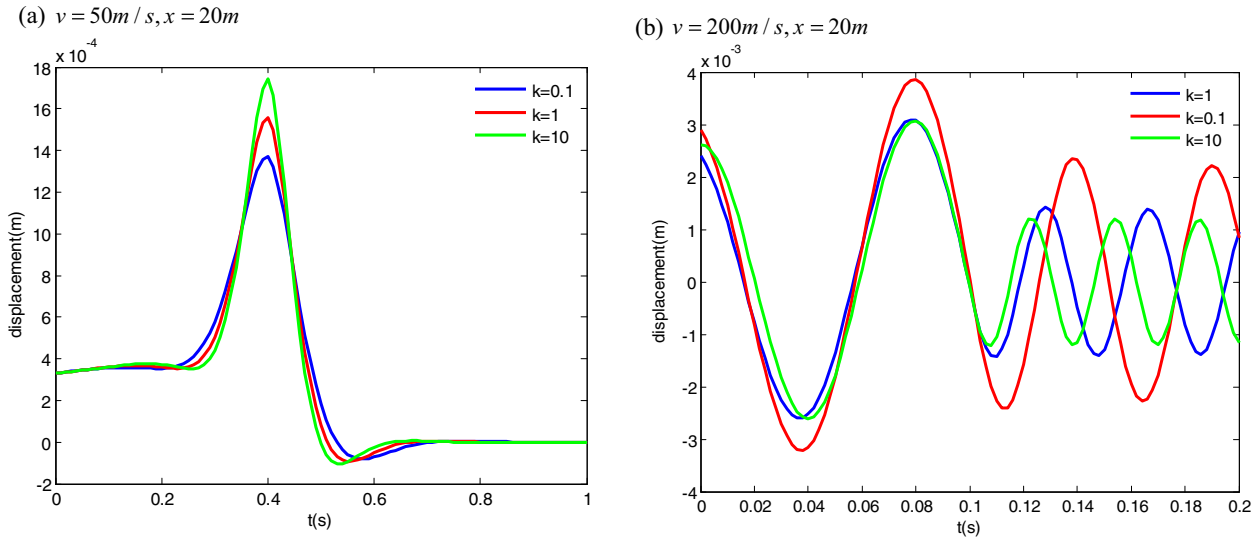

Fig. 12. Displacement response of upper beam in time domain: (a) $v = 50$ m/s,$x = 20$ m (b)$v = 200$ m/s,$x = 20$ m.

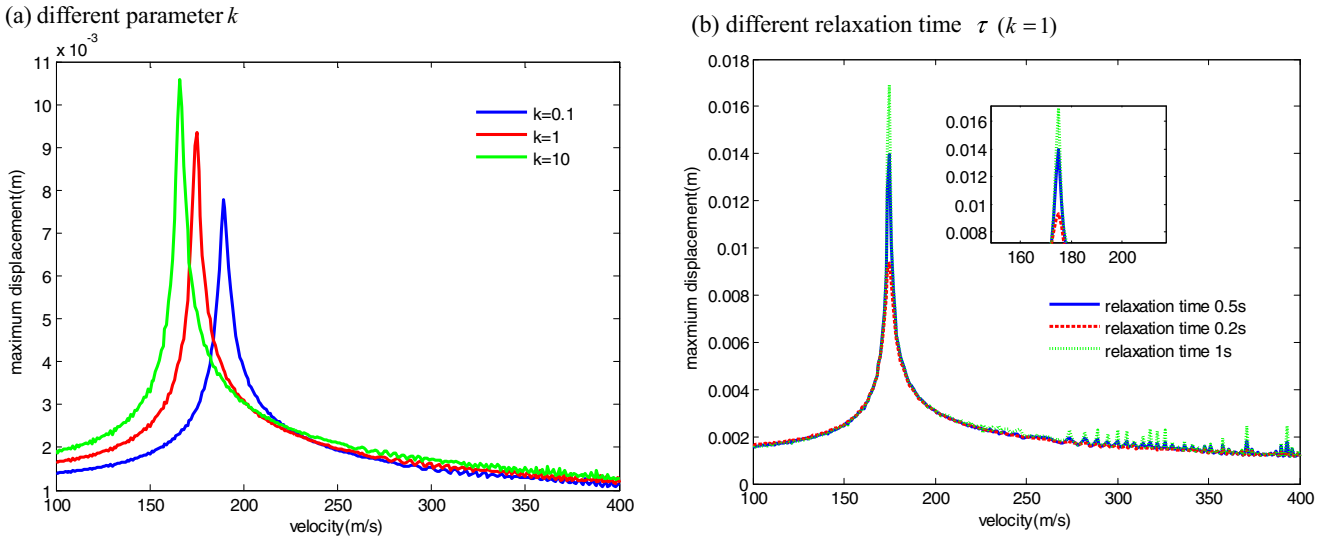

Fig. 13. Maximum track vibration displacement corresponding to different moving speeds.

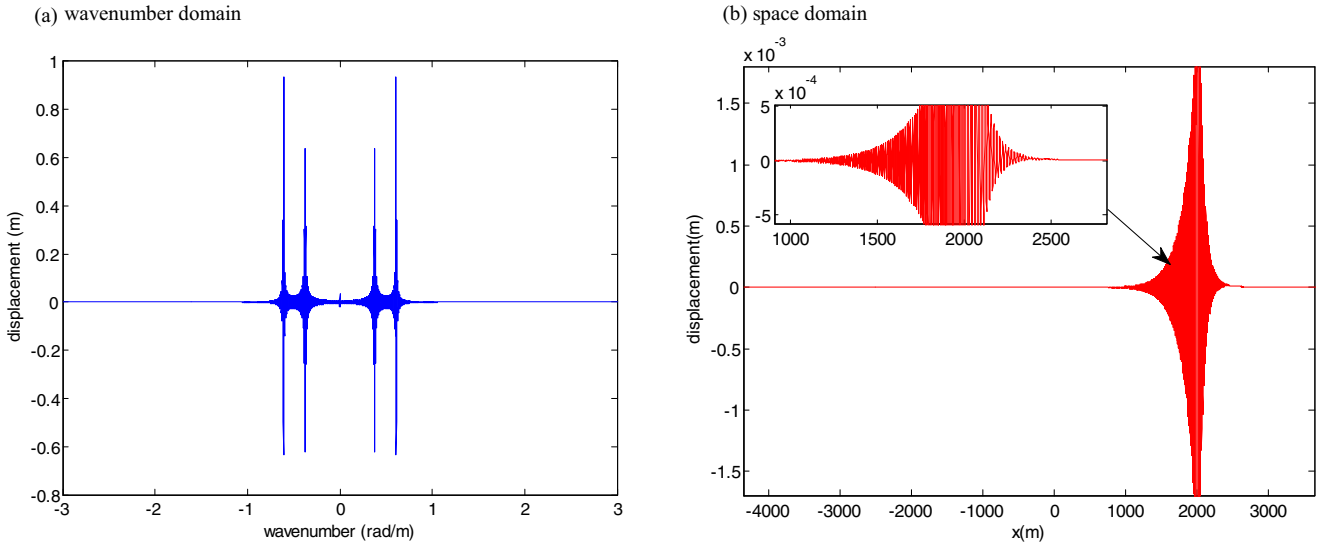

Fig. 14. Transverse displacement response of upper beam ($v = 200$ m/s,$k = 0.1, t = 10$ s): (a) wavenumber domain (b) space domain.

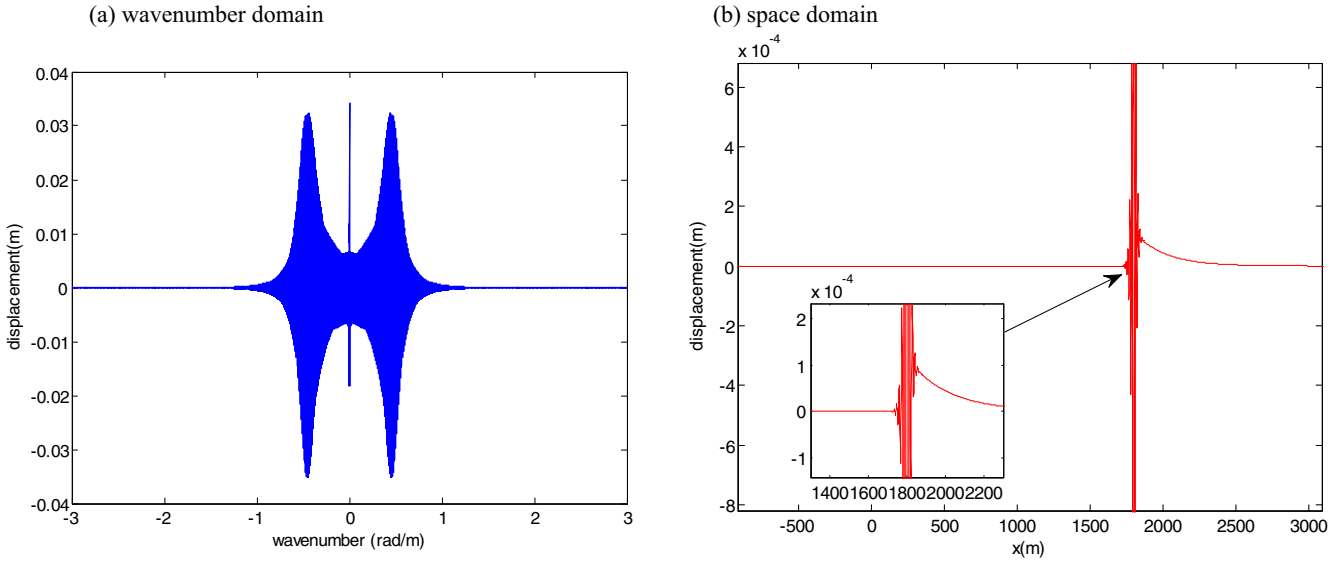

Fig. 15. Transverse displacement response of upper beam ($v = 180$ m/s,$k = 0.1, t = 10$ s): (a) wavenumber domain (b) space domain.

Fig. 13 shows maximum transverse displacement of upper beam corresponding to different speeds, where peaks of curves represent critical speed. As we can see from the Fig. 13(a), when the moving speed approximates critical speed of the track, amplitude of structure will increase sharply. Meanwhile, with the increase of the gradient k, critical speed will increase significantly, and the vibration amplitude will decrease. In Fig. 13(b), it is found that relaxation time τ only affects the value of peak, while it has no effect on the critical speed. Figs. 14 and 15 present transverse displacement response of upper beam, where Fig. 15a and b represent response in wavenumber domain and space domain respectively. According to Fig. 15, the critical speed of track is 189 m/s when $k = 0.1$. Therefore, the range of response is relatively narrow when moving speed less than critical speed. In comparison, track will vibrate in large spatial range as show in Fig. 14b when moving speed (200 m/s) exceeds critical speed.

4. Conclusion

In this paper, To acquire exact solutions of double-functionally graded Timoshenko beam system on Winkler-Pasternk elastic foundation, which are benchmarks in the field of engineering, the exact dynamic stiffness matrix of the double-functionally graded Timoshenko beam system on Winkler-Pasternak foundation under axial loading is established. The results obtained by dynamic stiffness method are in great agreement with previous studies. Thus, the correctness and effectiveness of the method was demonstrated. After comprehensive study of this beam system, we can conclude that:

1. With the increase of gradient parameter k, the fundamental frequency of the two-beam system decreases under different boundary conditions.
2. The stiffness of connecting layer has great influence on the reverse modes of two beams, and the increase of the stiffness can significantly increase the frequencies of the two-beam system.
3. the increase of the parameters of elastic foundation will increase the frequencies of two beam system and the effects of Winkler layer and shear layer on fundamental frequency are close.
4. The damping factor of connecting layer has great influence on the FRF, with the increase of the damping factor, the peaks of the FRF will decrease. And damping factor greatly affects the frequencies of reverse modes.
5. The increase of gradient parameter k can increase the loss factor of the two-beam system.
6. The buckling load decreases with the increase of the gradient parameter k under different boundary conditions.

References

[1] Loy CT, Lam KY, Reddy JN. Vibration of functionally graded cylindrical shells. Int J Mech Sci 1999;41:309–24.
[2] Reddy JN. Analysis of functionally graded plates. Int J Numer Meth Eng 2000;47:663–84.
[3] Cheng ZQ, Batra RC. Exact correspondence between eigenvalues of membranes and functionally graded simply supported polygonal plates. J Sound Vib 2000;229:879–95.
[4] Wu XH, Chen CQ, Shen YP. A high order theory for functionally graded piezoelectric shells. Int J Solids Struct 2002;39:5325–44.
[5] Javaheri R, Eslami MR. Thermal buckling of functionally graded plates. AIAA J 2002;40:162–9.
[6] Mian MA, Spencer AJM. Exact solutions for functionally graded laminated elastic materials. J Mech Phys Solids 1998;46:2283–95.
[7] Alshorbagy AE, Eltaher MA, Mahmoud FF. Free vibration characteristics of a functionally graded beam by finite element method. Appl Math Model 2011;35:412–25.
[8] Xiang HJ, Yang J. Free and vibration of a laminated FGM Timoshenko beam of variable thickness under heat conduction. Compos B Eng 2008;39:292–303.
[9] Zhu H, Sankar BV. A combined Fourier series-Galerkin method for the analysis of functionally graded beams. J Appl Mech Trans ASME 2004;71:421–4.
[10] Su H, Banerjee JR. Development of dynamic stiffness method for free vibration of functionally graded Timoshenko beams. Comput Struct 2015;147:107–16.
[11] Thai HT, Vo TP. Bending and free vibration of functionally graded beams using various higher-order shear deformation beam theories. Int J Mech Sci 2012;62:57–66.
[12] Lai SK, Harrington J, Xiang Y, Chow KW. Accurate analytical perturbation approach for large amplitude vibration of functionally graded beams. Int J Non-Linear Mech 2012;47:473–80.
[13] Huang Y, Li XF. A new approach for free vibration analysis of axially functionally graded beams with non-uniform cross-section. J Sound Vib 2010;329:2291–303.
[14] Lee SY, Kes HY. Free vibration of non-uniform beams resting on two-parameter elastic foundation with general elastic end restraints. Comput Struct 1990;34:421–9.
[15] Wang CM, Lam KY, He XQ. Exact solutions of Timoshenko beams on elastic foundation using Green's functions. Mech Struct Mach 1998;26:101–13.
[16] De Rosa MA, Maurizi MJ. The influence of concentrated masses and pasternak soil on the free vibration of Euler beams-exact solution. J Sound Vib 1998;212:573–81.

[17] Chen WQ, Lu CF, Bian ZG. A mix method for bending and free vibration of beams resting on a Pasternak elastic foundation. Appl Math Model 2004;28:877–90.
[18] Ying J, Lu CF, Chen WQ. Two-dimensional elasticity solutions fro functionally graded beams resting on elastic foundations. Compos Struct 2008;84:209–19.
[19] Bourada M, Kaci A, Houari MSA, Tounsi A. A new simple shear and normal deformations theory for functionally graded beams. Steel Compos Struct 2015;18(2):409–23.
[20] Hebali H, Tounsi A, Houari MSA, Bessaim A, Bedia EAA. A new quasi-3D hyperbolic shear deformation theory for the static and free vibration analysis of functionally graded plates. ASCE J Eng Mech 2014;140:374–83.
[21] Bennoun M, Houari MSA, Tounsi A. A novel five variable refined plate theory for vibration analysis of functionally graded sandwich plates. Mech Adv Mater Struct 2014;23(4):423–31.
[22] Yahia SA, Atmane HA, Houari MSA, Tounsi A. Wave propagation in functionally graded plates with porosities using various higher-order shear deformation plate theories. Struct Eng Mech 2015;53(6):1143–65.
[23] Belabed Z, Houari MSA, Tounsi A, Mahmoud SR, Bég OA. An efficient and simple higher order shear and normal deformation theory for functionally graded material (FGM) plates. Compos: Part B 2014;60:274–83.
[24] Mahi A, Adda Bedia EA, Tounsi A. A new hyperbolic shear deformation theory for bending and free vibration analysis of isotropic, functionally graded, sandwich and laminated composite plates. Appl Math Model 2015;39:2489–508.
[25] Hamidi A, Houari MSA, Mahmoud SR, Tounsi A. A sinusoidal plate theory with 5-unknowns and stretching effect for thermomechanical bending of functionally graded sandwich plates. Steel Compos Struct 2015;18:235–53.
[26] Kukla S. Free vibration of the system of two beams connected by many translational springs. J Sound Vib 1994;172:130–5.
[27] Oniszczuk Z. Free transverse vibrations of elastically connected simply supported double-beam complex system. J Sound Vib 2000;232:387–403.
[28] Aida T, Toda S, Ogawa N, Imada Y. Vibration control of beams by beam-type dynamic vibration absorbers. J Eng Mech 1992;118:248–58.
[29] Hussein MFM, Hunt HEM. Modelling of floating-slab tracks with continuous slabs under oscillating moving loads. J Sound Vib 2006;297:37–54.
[30] Shamalta M, Metrikine AV. Analytical study of the dynamic response of an embedded railway track to a moving load. Arch Appl Mech 2003;73:131–46.
[31] Zhang YQ, Lu Y, Wang SL, Liu X. Vibration and buckling of a double-beam system under compressive axial loading. J Sound Vib 2008;318:341–52.
[32] Li Jun, Chen Yong, Hua Hongxing. Exact dynamic stiffness matrix of a Timoshenko three-beam system. Int J Mech Sci 2008;50:1023–34.
[33] Ariei A, Ziaei-Rad S, Ghayour M. Transverse vibration of a multiple-Timoshenko beam system with intermediate elastic connections due to a moving load. Arch Appl Mech 2011;81:263–81.
[34] Simsek M. Nonlocal effects in the forced vibration of an elastically connected double-carbon nanotube system under a moving nanoparticle. Comput Mater Sci 2011;50:2112–23.
[35] Palmeri A, Adhikari S. A Galerkin-type state-space approach for transverse vibrations of slender double-beam systems with viscoelastic inner layer. J Sound Vib 2011;330:6372–86.
[36] Abu-Hilal M. Dynamic response of a double Euler-Bernoulli beam to a moving constant load. J Sound Vib 2006;297:477–91.
[37] Chen W-R. Bending vibration of axially loaded Timoshenko beams with locally distributed Kelvin-Voigt damping. J Sound Vib 2011;330:3040–56.
[38] Simsek Mesut, Cansiz Sinan. Dynamic of elastically connected double-functionally graded beam systems with different boundary conditions under action of a moving harmonic load. Compos Struct 2012;94:2861–78.
[39] Bouderba B, Houari MSA, Tounsi A, Bouderba B, Houari MSA. Thermomechanical bending response of FGM thick plates resting on Winkler-Pasternak elastic foundations. Steel Compos Struct 2013;14(1):85–104.
[40] Meziane MAA, Abdelaziz HH, Tounsi A. An efficient and simple refined theory for buckling and free vibration of exponentially graded sandwich plates under various boundary conditions. J Sandwich Struct Mater 2014;16(3):293–318.
[41] Zidi M, Tounsi A, Houari MSA, Bedia EAA, Bég OA. Bending analysis of FGM plates under hygro-thermo-mechanical loading using a four variable refined plate theory. Aerosp Sci Technol 2014;34:24–34.
[42] Duc ND. Nonlinear dynamic response of imperfect eccentrically stiffened FGM double curved shallow shells on elastic foundation. Compos Struct 2013;102:306–14.
[43] Duc ND, Quan TQ. Nonlinear stability analysis of double curved shallow FGM panel on elastic foundation in thermal environments. Mech Compos Mater 2012;48:435–48.
[44] Tung HV, Duc ND. Nonlinear response of shear deformable FGM curved panels resting on elastic foundations and subjected to mechanical and thermal loading conditions. Appl Math Model 2014;38:2848–66.
[45] Duc ND, Quan TQ. Nonlinear response of imperfect eccentrically stiffened FGM cylindrical panels on elastic foundation subjected to mechanical loads. Eur J Mech – A/Solids 2014;46:60–71.
[46] Duc ND, Thang PT. Nonlinear response of imperfect eccentrically stiffened ceramic-metal-ceramic FGM circular cylindrical shells surrounded on elastic foundations and subjected to axial compression. Compos Struct 2014;110:200–6.
[47] Duc ND, Tuan ND, Quan TQ, Quyen NV, Anh TV. Nonlinear mechanical, thermal and thermo-mechanical postbuckling of imperfect eccentrically stiffened thin FGM cylindrical panels on elastic foundations. Thin-Walled Struct 2015;96:155–68.
[48] Duc ND, Cong PH, Anh VM, Quang VD, Phuong Tran, Tuan ND, Thinh NH. Mechanical and thermal stability of eccentrically stiffened functionally graded conical shell panels resting on elastic foundations and in thermal environment. Compos Struct 2015;132:597–609.
[49] Duc ND. Nonlinear thermal dynamic analysis of eccentrically stiffened S-FGM circular cylindrical shells surrounded on elastic foundations using the Reddy's third-order shear deformation shell theory. Eur J Mech – A/Solids 2016;58:10–30.
[50] Duc ND. Nonlinear thermo-electro-mechanical dynamic response of shear deformable piezoelectric Sigmoid functionally graded sandwich circular cylindrical shells on elastic foundations. J Sandwich Struct Mater 2016.
[51] Kolousek V. Anwendung des Gesetzes der virtuellen Ver schiebungen und des Reziprozitatssatzes in der Stabwerksdy nam ik Ingenieur Archiv 1941;21:340–63.
[52] Banerjee JR. Coupled bending torsional dynamic stiffness matrix for beam elements. Int J Numer Meth Eng 1989;28:1283–9.
[53] Banerjee JR, Fisher SA. Coupled bending-torsional dynamic stiffness matrix for axially loaded beam elements. Int J Numer Meth Eng 1992;33:739–51.
[54] Banerjee JR, Williams FW. Coupled bending torsional dynamic stiffness matrix for Timoshenko beam elements. Comput Struct 1992;42:301–10.
[55] Jun Li, Rongying Shen, Hongxing Hua. Coupled bending and torsional vibration of axially loaded bernoulli euler beams including warping effects. Appl Acoust 2004;65:153–70.
[56] Banerjee JR, Williams FW. Coupled bending torsional dynamic stiffness matrix of an axially loaded timoshenko beam element. Int J Solids Struct 1994;31:749–62.
[57] Banerjee JR, Williams FW. Exact Bernoulli Euler dynamic stiffness matrix for a range of tapered beams. Int J Numer Meth Eng 1985;21:2289–302.
[58] Leung AYT, Zhou WE. Dynamic stiffness analysis of non-uniform timoshenko beams. J Sound Vib 1995;181:447–56.
[59] Wittrick WH, Williams FW. A general algorithm for computing natural frequencies of elastic structures. Q J Mech Appl Mech 1971;24:263–84.
[60] Si Yuan, Kangsheng Ye, Williams FW, Kennedy D. Recursive second order convergence method for natural frequencies and modes when using dynamic stiffness matrices. Int J Numer Meth Eng 2003;56:152–62.
[61] Arikoglu Aytac, Ozkol Ibrahim. Vibration analysis of composite sandwich beams with viscoelastic core by using differential transform method. Compos Struct 2010;92:3031–9.
[62] Tan SJ, Wu ZG, Zhong WX. Adaptive selection of parameters for precise computation of matrix exponential based on Pade′ approximation. Chin J Theor Appl Mech 2009;41:961–6.